

# Nuclear composition of gamma-ray burst fireballs

Andrei M. Beloborodov<sup>1,2,3</sup>

## ABSTRACT

We study three processes that shape the nuclear composition of the fireballs in gamma-ray bursts (GRBs): (1) neutronization in the central engine, (2) nucleosynthesis in the fireball as it expands and cools, and (3) spallation of nuclei in subsequent internal shocks. The fireballs are shown to have a neutron excess and a marginally successful nucleosynthesis. They are composed of free nucleons,  $\alpha$ -particles, and deuterium. A robust result is the survival of a significant neutron component, which has important implications. First, as shown in previous works, neutrons can lead to observable multi-GeV neutrino emission. Second, as we show in an accompanying paper, the neutrons impact the explosion dynamics at radii up to  $10^{17}$  cm and change the mechanism of the GRB afterglow emission.

*Subject headings:* accretion, accretion disks — cosmology: miscellaneous — dense matter — gamma rays: bursts — nuclear reactions, nucleosynthesis

## 1. Introduction

The phenomenon of a gamma-ray burst (GRB) is generated by a compact, dense, and energetic engine (see Mészáros 2002 for a review). The mass of the central engine is a few  $M_\odot$ , its size is  $10^6 - 10^7$  cm, and it has a blackbody temperature  $kT \gtrsim 1$  MeV. The dense and hot baryonic matter is composed of free nucleons, and it is partially ejected in a highly relativistic wind (fireball). The initial nuclear composition and its evolution during expansion of the fireball turn out crucial for the explosion physics. In particular, a neutron component is likely to survive and affect the observed explosion (Derishev, Kocharovsky, & Kocharovsky 1999). Recent works on neutrons (Bahcall & Mészáros 2000; Mészáros & Rees 2000; Fuller, Puet, & Abazajian 2000; Puet, Abazajian, & Fuller 2001; Puet & Dalal 2002; Bulik, Sikora, & Moderski 2002) focused on relative motion of the neutron and ion components, which can lead to observable multi-GeV neutrino emission. In an accompanying paper (Beloborodov 2002, Paper II) we show that the neutrons also profoundly change the mechanism of the GRB afterglows.

---

<sup>1</sup>Canadian Institute for Theoretical Astrophysics, 60 St. George Street, Toronto, ON M5S 3H8, Canada

<sup>2</sup>Physics Department, Columbia University, 538 West 120th Street New York, NY 10027

<sup>3</sup>Astro-Space Center of Lebedev Physical Institute, Profsojuznaja 84/32, Moscow 117810, Russia

In the present paper, we study in detail the processes that shape the nuclear composition of the fireballs, with an emphasis on the neutron component. In § 2, we assess the production of neutrons by the central engine and the resulting neutron-to-proton ratio in the ejected material (scale  $R \sim r_0 < 10^7$  cm). In § 3, we calculate nucleosynthesis at the early stage of the explosion and the abundances of survived free nucleons and synthesized helium ( $R = 10^7 - 10^9$  cm). Similar nucleosynthesis calculations, with different codes, have been done recently by Lemoine (2002) and Pruet, Guiles, & Fuller (2002). In § 4, we study spallation of helium at later stages when internal motions develop in the ejecta ( $R = 10^9 - 10^{12}$  cm). The subsequent dynamics of GRB blast waves with the survived neutron component ( $R = 10^{15} - 10^{17}$  cm) is investigated in Paper II.

## 2. Neutron Excess

There are various models for the central engines of GRBs. It may be a young neutron star whose rotational energy is emitted in a magnetized wind, a neutron star merger, or a massive star collapse. The latter two scenarios proceed via formation of a black hole of mass  $M \sim M_\odot$  and subsequent disk-like accretion of a comparable mass. The baryonic component of the ejected fireball is then picked up from the accretion disk.

The central engines are sufficiently dense for the electron capture reaction. We will calculate at what densities and temperatures this process creates a neutron excess (neutron-to-proton ratio above unity), and then show that the GRB engines are likely to satisfy these conditions. We will illustrate with the accretion-type models of GRBs, where the matter density can be relatively low and neutronization is most questionable. Even in this case neutronization does happen and the ejected baryons should have a neutron excess.

### 2.1. The equilibrium $Y_e$

Consider a dense,  $\rho > 10^7$  g cm $^{-3}$ , and hot,  $kT > m_e c^2$ , matter. The rates of photon emission and absorption are huge and the matter is filled with Planckian radiation. Also, the rates of  $e^\pm$  pair creation and annihilation ( $\gamma + \gamma \leftrightarrow e^- + e^+$ ) are huge, and the pairs are in perfect thermodynamic equilibrium with the baryonic matter and radiation. The  $e^\pm$  number densities are

$$n_\pm = \frac{(m_e c)^3}{\pi^2 \hbar^3} \int_0^\infty f_\pm(\sqrt{p^2 + 1}) p^2 dp. \quad (1)$$

Here  $p$  is particle momentum in units of  $m_e c$  and  $f_\pm$  is the Fermi-Dirac occupation function,

$$f_\pm(x) = \frac{1}{\exp[(x \pm \mu)/\theta] + 1}, \quad (2)$$

where  $\mu \equiv \mu_- = -\mu_+$  is the electron chemical potential in units of  $m_e c^2$ , and  $\theta = kT/m_e c^2$ . (Thermodynamic equilibrium of  $e^\pm$  with radiation implies  $\mu_+ + \mu_- = 0$ .) In addition to equation (1),

we have the charge-neutrality condition,

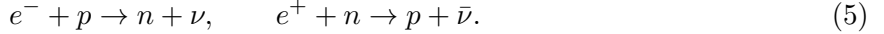
$$n_- - n_+ = Y_e \frac{\rho}{m_p}, \quad (3)$$

where  $Y_e$  is the proton-to-nucleon ratio, which would equal the electron-to-nucleon ratio in the absence of  $e^\pm$  pairs. Equations (1) and (3) determine  $\mu$  and  $n_\pm$  for given  $T$ ,  $\rho$ , and  $Y_e$ . The electrons become degenerate if  $\mu$  exceeds  $\theta$ , which happens below the characteristic degeneracy temperature,

$$\theta_{\text{deg}} = \frac{\hbar}{m_e c} \left( \frac{\rho}{m_p} \right)^{1/3}, \quad kT_{\text{deg}} = 7.7 \left( \frac{\rho}{10^{11} \text{ g cm}^{-3}} \right)^{1/3} \text{ MeV.} \quad (4)$$

Degeneracy exponentially suppresses the positron density,  $n_+ / n_- \approx \exp(-\mu/\theta)$ , because  $e^\pm$  are created only above the Fermi energy level,  $E_F = \mu$ , in the exponential tail of the thermal distribution.

At temperatures and densities under consideration, the baryonic matter is in nuclear statistical equilibrium, and it is dominated by free nucleons in the unshadowed region of Figure 1. The boundary of this region has been calculated with the Lattimer-Swesty Equation of State code (Lattimer & Swesty 1991). The free protons and neutrons can capture  $e^-$  and  $e^+$  via charged current reactions,



These reactions can rapidly convert protons into neutrons and neutrons back into protons, and establish an equilibrium  $Y_e = n_p / (n_n + n_p)$ , where  $n_p$  and  $n_n$  are number densities of protons and neutrons, respectively.<sup>4</sup> We now calculate the equilibrium  $Y_e(T, \rho)$ , and in § 2.2 we will show how it applies to the GRB central engines.

The exact equilibrium  $Y_e$  depends on whether the opposite reactions — reabsorption of the emitted  $\nu$  and  $\bar{\nu}$  — also operate in the flow. We first consider the  $\nu$ -transparent case, where reabsorption can be neglected, and then address the  $\nu$ -opaque case.

### 2.1.1. Neutrino-transparent matter

The rates of  $e^-$  and  $e^+$  capture can be derived from the standard electro-weak theory (e.g., Bruenn 1985). We assume the nucleons to be non-degenerate, and then the rates are

$$\dot{n}_{e^-p} = 6.3 \times 10^{-4} n_p \int_0^\infty f_-(\omega + Q) (\omega + Q)^2 \left[ 1 - \frac{1}{(\omega + Q)^2} \right]^{1/2} \omega^2 d\omega \text{ cm}^{-3} \text{ s}^{-1}, \quad (6)$$

$$\dot{n}_{e^+n} = 6.3 \times 10^{-4} n_n \int_{Q+1}^\infty f_+(\omega - Q) (\omega - Q)^2 \left[ 1 - \frac{1}{(\omega - Q)^2} \right]^{1/2} \omega^2 d\omega \text{ cm}^{-3} \text{ s}^{-1}, \quad (7)$$

---

<sup>4</sup>The neutron decay  $n \rightarrow p + e^- + \nu$  is a slow process on GRB timescales and it is neglected here.

where  $\omega$  is neutrino energy in units of  $m_e c^2$  and  $Q = (m_n - m_p)/m_e = 2.53$ . An equilibrium  $Y_e$  is established when the rates of  $e^-$  and  $e^+$  captures are equal,<sup>5</sup>

$$\dot{n}_{e^+n} = \dot{n}_{e^-p}. \quad (8)$$

Equations (1), (3), and (8) determine  $Y_e$  for given  $\rho$  and  $T$ . Contours of function  $Y_e(\rho, T)$  on the  $\rho - T$  plane are shown in Figure 1. The n/p-ratio equals  $(1 - Y_e)/Y_e$ , and the neutrons dominate over protons where  $Y_e < 0.5$ .

At mild degeneracy,  $\mu < \theta$ , and high temperatures,  $\theta > 1$ , the equilibrium  $Y_e$  can be derived analytically. The capture rates then read

$$\dot{n}_{e^-p} = 6.3 \times 10^{-4} n_p \theta^5 \left[ \frac{45}{2} \zeta(5) + \frac{7\pi^4}{120} \frac{(2\mu - Q)}{\theta} \right] \text{ cm}^{-3} \text{ s}^{-1}, \quad (9)$$

$$\dot{n}_{e^+n} = 6.3 \times 10^{-4} n_n \theta^5 \left[ \frac{45}{2} \zeta(5) - \frac{7\pi^4}{120} \frac{(2\mu - Q)}{\theta} \right] \text{ cm}^{-3} \text{ s}^{-1}, \quad (10)$$

where  $\zeta(5) = 1.037$  is Riemann  $\zeta$ -function. We neglected here next-order terms  $O(Q^2/\theta^2)$ ,  $O(\mu^2/\theta^2)$ , and  $O[(Q + 1)^5/\theta^5]$ , and used the formula  $\int_0^\infty (e^x + 1)^{-1} x^n dx = (1 - 2^{-n})\Gamma(n + 1)\zeta(n + 1)$  with  $\Gamma(n + 1) = n!$  for integer  $n$ . Equating the two rates, we get the equilibrium  $Y_e = n_p/(n_n + n_p)$ ,

$$Y_e = \frac{1}{2} + \frac{7\pi^4}{1350\zeta(5)} \frac{(Q/2 - \mu)}{\theta} = \frac{1}{2} + 0.487 \frac{(Q/2 - \mu)}{\theta}. \quad (11)$$

In the non-degenerate limit,  $\mu \rightarrow 0$ , this gives  $Y_e = 0.5 + 0.62/\theta > 0.5$  and implies a proton excess, which is due to the positive difference  $Q$  between the neutron and proton mass. A very mild degeneracy  $\mu = Q/2 < \theta$  is sufficient to drive  $Y_e$  below 0.5. This happens because the  $e^+$  density decreases, and the  $e^-$  capture becomes preferential. It is instructive to write the  $e^-$  and  $e^+$  densities using the linear expansion of equation (1) in  $\mu/\theta$ ,

$$n_{\pm} = \frac{1}{\pi^2 \lambda^3} \left[ \frac{3}{2} \zeta(3) \theta^3 \mp \frac{\pi^2}{6} \mu \theta^2 \right], \quad \mu < \theta, \quad (12)$$

where  $\lambda = \hbar/m_e c = 3.862 \times 10^{-11}$  cm and  $\zeta(3) = 1.202$ . Then  $n_- - n_+ = n_p$  yields

$$\mu = 3Y_e \frac{\lambda^3 \rho}{m_p \theta^2}. \quad (13)$$

The condition  $\mu > Q/2$  that defines the neutron-excess region on the  $T - \rho$  plane ( $Y_e < 0.5$ ) can be written as  $\theta < \theta_n(\rho)$ , where

$$\theta_n = \left( \frac{3\lambda^3 \rho}{Q m_p} \right)^{1/2}, \quad kT_n = 33 \left( \frac{\rho}{10^{11}} \right)^{1/2} \text{ MeV}. \quad (14)$$

---

<sup>5</sup>In the  $\nu$ -transparent regime, the neutrinos are sometimes prescribed a zero chemical potential. In fact, the balance of chemical potentials  $\mu_p + \mu = \mu_n + \mu_\nu = \mu_n$  is *not* established, because the neutrinos are out of thermodynamic equilibrium. This condition holds only in the cold limit  $T \rightarrow 0$  (Landau & Lifshitz 1980), and it is approximately valid in the strongly degenerate regime,  $\theta < \mu$ .

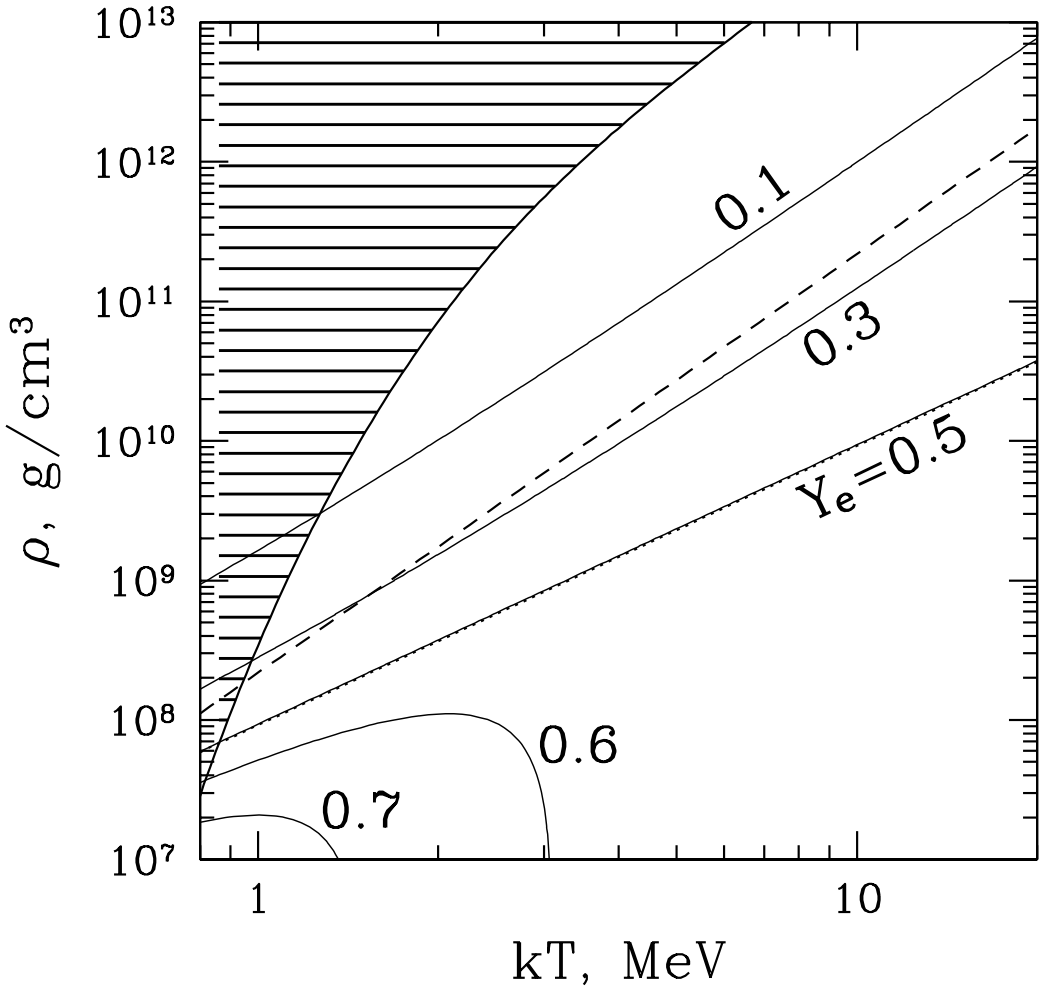


Fig. 1.— Contours of the equilibrium  $Y_e(T, \rho)$  on the  $T - \rho$  plane for  $\nu$ -transparent matter. Dashed line shows the degeneracy temperature (eq. 4). In the shadowed region, the baryonic matter is dominated by composite nuclei, and the calculations based on rates (6) and (7) are not valid. The analytically calculated boundary  $Y_e = 0.5$  (eq. 14) is also plotted here by a dotted line, which perfectly coincides with the numerically found contour  $Y_e = 0.5$ .

This simple formula perfectly coincides with the numerical results (Fig. 1). That a very mild electron degeneracy is sufficient to create a neutron excess can also be seen by comparing  $T_n$  with  $T_{\text{deg}}$ ,

$$\frac{T_n}{T_{\text{deg}}} \approx 4.3 \left( \frac{\rho}{10^{11}} \right)^{1/4}. \quad (15)$$

A useful explicit formula for the equilibrium  $Y_e(T, \rho)$  in  $\nu$ -transparent matter with mild degeneracy is derived from equations (11) and (13),

$$Y_e(\theta, \rho) = \frac{1}{2} \left( 1 + \frac{1.232}{\theta} \right) \left( 1 + 1.436 \frac{\lambda^3 \rho}{m_p \theta^3} \right)^{-1}. \quad (16)$$

It agrees with the numerical calculations shown in Figure 1 with a high accuracy,  $\delta Y_e / Y_e < 1\%$  at  $Y_e > 0.35$ . In a more degenerate region,  $Y_e < 0.35$ , the formula can still be used, though its error increases to 10% at  $Y_e = 0.2$  and 29% at  $Y_e = 0.1$ .

### 2.1.2. Neutrino-opaque matter

If the matter is opaque to neutrinos, a complete thermodynamic equilibrium is established. The detailed balance now holds,  $e^- + p \leftrightarrow n + \nu$  and  $e^+ + n \leftrightarrow p + \bar{\nu}$ , and the equilibrium  $Y_e$  is determined by the condition

$$\mu + \mu_p = \mu_n + \mu_\nu, \quad (17)$$

where  $\mu$ ,  $\mu_p$ ,  $\mu_n$ , and  $\mu_\nu$  are chemical potentials (in units of  $m_e c^2$ ) of the electrons, protons, neutrons, and neutrinos, respectively, all including the particle rest mass-energy. The antineutrinos have chemical potential  $\mu_{\bar{\nu}} = -\mu_\nu$ , so that  $\mu_n + \mu_+ = \mu_p + \mu_{\bar{\nu}}$  is also satisfied. The neutrons and protons have a Maxwellian distribution, which gives  $n_n n_p^{-1} = \exp[(\mu_n m_e c^2 - m_n c^2)/kT] \exp[(-\mu_p m_e c^2 + m_p c^2)/kT]$  and

$$\mu_n - \mu_p = \theta \ln(n_n/n_p) + Q. \quad (18)$$

The thermalized  $\nu$  and  $\bar{\nu}$  obey Fermi-Dirac statistics, and they are described in the same way as  $e^\pm$  (see eqs. [1] and [2]). The only difference is that the statistical weight of energy states is one for neutrinos and two for electrons. The neutrino chemical potential must vanish if  $\nu$  and  $\bar{\nu}$  have equal densities,  $n_\nu = n_{\bar{\nu}}$ . A changing  $Y_e$ , however, implies that the matter emits non-equal numbers of  $\nu$  and  $\bar{\nu}$ , and then  $n_\nu \neq n_{\bar{\nu}}$  and  $\mu_\nu \neq 0$ .

Suppose  $N_\nu$  neutrinos and  $N_{\bar{\nu}}$  anti-neutrinos have been emitted per nucleon. This causes a change of  $Y_e$ ,

$$Y_e - Y_e^0 = N_{\bar{\nu}} - N_\nu, \quad (19)$$

where  $Y_e^0$  is an initial value that matter had before the neutrino emission. If all the emitted neutrinos remain trapped in the matter,  $(n_\nu - n_{\bar{\nu}})/n_b = Y_e - Y_e^0$ , where  $n_b = n_n + n_p$  is the total nucleon density. In fact, even if the neutrinos are reabsorbed, they may still diffuse out of the

matter quickly, so that a fraction  $x$  of neutrinos can be lost. Then,  $(n_\nu - n_{\bar{\nu}})/n_b = (1 - x)(Y_e - Y_e^0)$  and

$$\frac{n_\nu - n_{\bar{\nu}}}{n_- - n_+} = (1 - x) \left( 1 - \frac{Y_e^0}{Y_e} \right). \quad (20)$$

At  $x \rightarrow 1$  (efficient neutrino cooling) we get  $|n_\nu - n_{\bar{\nu}}| \ll n_- - n_+$ , and the neutrino chemical potential can be neglected compared to that of the electrons. Thus, the chemical equilibrium in  $\nu$ -cooled,  $\nu$ -opaque matter reads

$$\mu = \theta \log(n_n/n_p) + Q. \quad (21)$$

Equation (21) combined with equations (1) and (3) determines an equilibrium  $Y_e$  as a function of  $T$  and  $\rho$ . Where heavy nuclei form, equation (18) is not valid. To cover this region on the  $T - \rho$  plane, we use the Lattimer-Swesty Equation of State code and compute  $\mu_n$  and  $\mu_p$  taking into account heavy nuclei. Then we find  $Y_e$  that satisfies  $\mu = \mu_n - \mu_p$ . The results are shown in Figure 2. Note that in the degenerate region  $T < T_{\text{deg}}$ , the results also approximately apply to the  $\nu$ -transparent equilibrium problem of § 2.1.1 and give  $Y_e$  in the shadowed region of Figure 1.

The neutron excess boundary,  $Y_e = 0.5$ , lies in the region where all nucleons are free and the electrons are mildly degenerate,  $\mu < \theta$ . Equation (21) shows that this boundary is defined by  $\mu = Q$ . Using the linear expansion in  $\mu/\theta$  (13), we get a simple equation for  $Y_e(\theta, \rho)$ ,

$$\frac{3Y_e \rho \lambda^3}{\theta^2 m_p} = \theta \log \left( \frac{1 - Y_e}{Y_e} \right) + Q, \quad (22)$$

and  $Y_e = 0.5$  corresponds to

$$\theta_n = \left( \frac{3\lambda^3 \rho}{2Qm_p} \right)^{1/2}, \quad kT_n = 23.1 \left( \frac{\rho}{10^{11}} \right)^{1/2} \text{ MeV}. \quad (23)$$

It coincides exactly with the contour  $Y_e = 0.5$  calculated with the Lattimer-Swesty code (Fig. 2). Note also that  $T_n = 3T_{\text{deg}}(\rho/10^{11})^{1/6}$ .

Finally, we address the regime when the neutrinos are not only thermalized but also trapped in the matter. It can happen in GRB accretion flows with high accretion rates,  $\dot{M} > 1M_\odot/\text{s}$  (e.g. Di Matteo, Perna, & Narayan 2002). Then  $\mu_\nu$  should not be neglected in the chemical balance. Let us find the neutron-excess boundary in this case. Like equation (13), we derive for neutrinos

$$\mu_\nu = \frac{3\lambda^3(n_\nu - \nu_{\bar{\nu}})}{2\theta^2}, \quad (24)$$

and substitute  $n_\nu - \nu_{\bar{\nu}} = (Y_e - Y_e^0)(\rho/m_p)$ . The chemical balance  $\mu_e - \mu_\nu = \mu_n - \mu_p$  now reads

$$\frac{3(Y_e + Y_e^0) \rho \lambda^3}{2\theta^2 m_p} = \theta \log \left( \frac{1 - Y_e}{Y_e} \right) + Q, \quad (25)$$

and  $Y_e = 0.5$  corresponds to

$$\theta_n = \left[ \frac{3(0.5 + Y_e^0)\lambda^3 \rho}{2Qm_p} \right]^{1/2}. \quad (26)$$

At  $Y_e^0 = 0.5$  it coincides with equation (23) as it should do, because  $Y_e = 0.5 = Y_e^0$  requires that  $\nu$  and  $\bar{\nu}$  are emitted in equal numbers and  $\mu_\nu = 0$ .

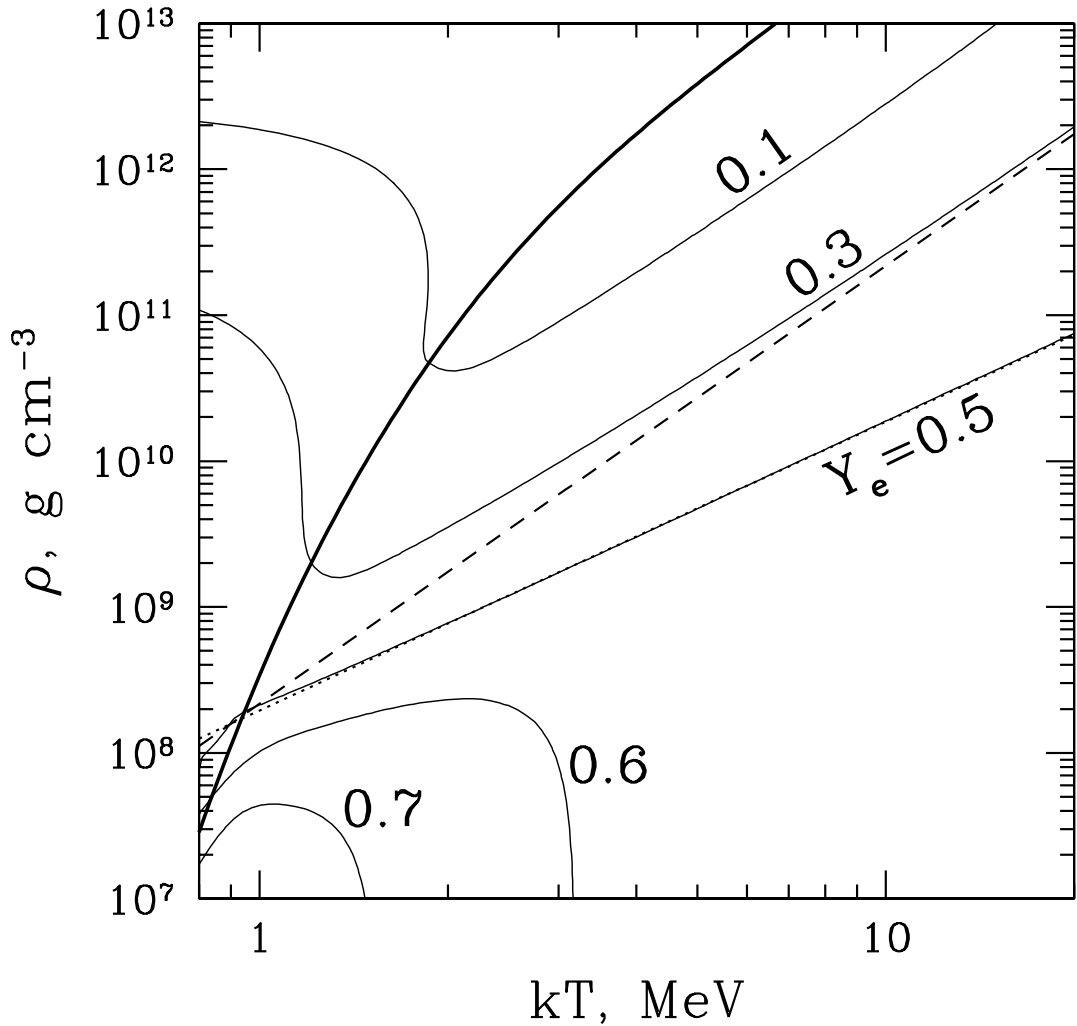


Fig. 2.— Contours of the equilibrium  $Y_e(T, \rho)$  on the  $T - \rho$  plane for  $\nu$ -opaque matter with  $\mu_\nu = 0$ . Dashed line shows the degeneracy temperature (eq. 4). Thick solid curve shows the boundary of the free-nucleon region (same as in Fig. 1). Above this curve, the composite nuclei dominate, which prefer equal numbers of neutrons and protons, and therefore the contours  $Y_e = \text{const}$  bend upward. The analytically calculated boundary  $Y_e = 0.5$  (eq. 23) is shown by the dotted line, which almost perfectly coincides with the numerically found contour  $Y_e = 0.5$ .

### 2.1.3. Effects of magnetic fields

Magnetic fields have been neglected in the above calculations, which is a valid approximation as long as the field does not affect the particle distribution functions. Magnetic fields can be generated in the GRB central engines by dynamo, and their energy is a fraction  $\epsilon_B < 1$  of the total energy density  $w$ , so that

$$B = \sqrt{8\pi\epsilon_B w}. \quad (27)$$

Here  $w$  includes the energy of baryons, radiation, and  $e^\pm$ ; it also includes the neutrino energy if the disk is  $\nu$ -opaque. The field has the strongest effect of light charged particles —  $e^\pm$ . It introduces the discrete energy levels (Landau & Lifshitz 1980),

$$\frac{E_j}{m_e c^2} = \left[ 1 + p_z^2 + 2j \frac{\hbar\Omega_B}{m_e c^2} \right]^{1/2}, \quad j = 0, 1, \dots \quad (28)$$

Here,  $-\infty < p_z < \infty$  is the component of the electron momentum parallel to the field, and  $\Omega_B = eB/m_e c$  is the cyclotron frequency. The magnetic field also changes the phase-space density factor in equation (1):  $p^2 dp$  is replaced by  $(\Omega_B \hbar / 2m_e c^2) dp_z$ . Both effects are important if  $(\Omega \hbar / m_e c^2) > p_z^2$ . The mean parallel momentum of the relativistic  $e^\pm$  equals  $\sqrt{3}kT/c$ , and the condition for the field effects to be important reads

$$\frac{\hbar\Omega_B}{m_e c^2} > 3\theta^2. \quad (29)$$

For any plausible  $\epsilon_B < 1$ , the magnetic field is important only where the electrons are degenerate, and the energy density  $w$  is dominated by either baryons,  $w_b = (3/2)kT\rho/m_p$ , or degenerate electrons,  $w_{\text{deg}} = (9/4)(\pi/3)^{4/3}Y_e m_e c^2 (\rho/m_p)^{4/3}$ . The condition (29) can be written as

$$\theta < \left( \frac{\rho \lambda^3}{m_p} \right)^{1/3} \times \begin{cases} \left( \frac{4\pi}{3} \alpha_f \epsilon_B \right)^{1/3} & \epsilon_B > (\pi^3 Y_e^3 / 32\alpha_f), \\ \left( \frac{\pi}{3} \right)^{7/12} (6Y_e \alpha_f \epsilon_B)^{1/4} & \epsilon_B < (\pi^3 Y_e^3 / 32\alpha_f). \end{cases} \quad (30)$$

where  $\alpha_f$  is the fine structure constant. The upper line corresponds to  $w_b > w_{\text{deg}}$  and the lower line to  $w_{\text{deg}} > w_b$ .

## 2.2. GRB central engines

There exists a general constraint on the electron degeneracy in the engine. Its derivation makes use of two facts: (1) The engine is gravitationally bound — otherwise it would explode, and baryon contamination of the fireball would be inevitable. GRB models normally envision a quasi-static engine that liberates a fraction of its gravitational binding energy and passes it to a tiny amount of mass outside the engine, thus creating a highly relativistic outflow. (2) The engine is compact (size  $r < 10^7$  cm), and it has a relativistic blackbody temperature  $\theta = kT/m_e c^2 > 1$ .

A gravitationally bound object has a sound speed smaller than the break-up velocity  $v = (GM/r)^{1/2}$ , where  $M$  is the object mass. It gives the constraint

$$\frac{P}{\rho} \lesssim 0.1c^2 \left( \frac{r}{3r_g} \right)^{-1}, \quad (31)$$

where  $r_g = 2GM/c^2$  is the gravitational radius of the object. Pressure  $P = P_\gamma + P_\pm + P_\nu + P_b$  includes contributions from radiation,  $e^\pm$ , neutrinos, and baryons. We have  $P_\gamma + P_\pm = (11/12)aT^4$  if the  $e^\pm$  are weakly degenerate, and a maximum  $P_\nu = (7/24)aT^4$  for each neutrino species if it is thermalized, where  $a = (\pi^2 k^4 / 15 \hbar^3 c^3) = 7.56 \times 10^{-15}$  erg cm<sup>-3</sup> K<sup>-4</sup> is the radiation constant. Approximately,

$$P \approx aT^4 + \frac{\rho}{m_p} kT. \quad (32)$$

It is easy to see that

$$\frac{aT^4}{(\rho/m_p)kT} = \frac{\pi^2}{15} \frac{\theta^3}{\theta_{\text{deg}}^3}. \quad (33)$$

The baryonic pressure gets dominant at  $\theta \sim \theta_{\text{deg}}$ , and at even lower temperatures,  $\theta < (\pi/4)Y_e\theta_{\text{deg}}$ , the pressure of degenerate electrons  $P_{\text{deg}} = (3/4)(\pi/3)^{4/3}Y_e m_e c^2 (\rho/m_p)^{4/3}$  takes over. We are interested now in the upper bound on  $\theta/\theta_{\text{deg}}$  and therefore consider  $\theta \gtrsim \theta_{\text{deg}}$  with  $P \approx aT^4$ . The constraint (31) then reads

$$\frac{\theta}{\theta_{\text{deg}}} \lesssim 2 \left( \frac{\rho}{10^{11}} \right)^{-1/12} \left( \frac{r}{3r_g} \right)^{-1/4}, \quad (34)$$

and also gives a lower bound on the electron chemical potential (eq. 13),

$$\frac{\mu}{Q} \gtrsim 5Y_e \left( \frac{\rho}{10^{11}} \right)^{1/2} \left( \frac{r}{3r_g} \right)^{1/2}. \quad (35)$$

We know from § 2.1 that the condition  $Y_e < 0.5$  reads  $\mu > Q/2$  for  $\nu$ -transparent matter and  $\mu > Q$  for the  $\nu$ -opaque matter. We now see that any engine of size  $r$  and density  $\rho > 10^{10}(r/3r_g)^{-1}$  g/cm<sup>3</sup> satisfies this condition and tends to an equilibrium  $Y_e < 0.5$ . This is evidently the case in specific models of neutron star mergers (Ruffert & Janka 1999), as well as magnetized neutron stars. The collapsar scenario (MacFadyen & Woosley 1999) invokes a relatively low-density accretion flow, and here neutronization is questionable. We therefore shall study accretion flows in more detail. We also need to check whether the equilibrium  $Y_e$  is achieved on the accretion timescale.

### 2.2.1. GRB accretion flows

All accretion models of the GRBs invoke rotation that creates a funnel along which the fireball can escape. The accretion flow is viewed as a rotating disk maintained in hydrostatic balance in the vertical direction, which gradually spirals into the central black hole. A standard model assumes turbulent viscosity in the disk with a stress tensor  $W_{r\phi} = \alpha c_s^2$ , where  $c_s = (P/\rho)^{1/2}$  is the isothermal

sound speed, and  $\alpha = 0.01 - 0.1$  (Balbus & Hawley 1998). Same stress tensor can be described in terms of a viscosity coefficient  $\nu = (2/3)\alpha c_s H$ , where  $H$  is the half-thickness of the disk.

The velocity of accretion at radius  $r$  is

$$u^r = W_{r\phi} \frac{\Omega_K}{rS}, \quad S(r) = 1 - \left(\frac{r_{\text{in}}}{r}\right)^{1/2}, \quad (36)$$

where  $\Omega_K(r) = (GM/r^3)^{1/2}$  is angular velocity of Keplerian rotation,  $M$  is the hole mass, and  $r_{\text{in}}$  is the inner boundary of the disk (the marginally stable orbit);  $r_{\text{in}} = 3r_g$  for non-rotating and  $r_{\text{in}} = r_g/2$  for extremely rotating black holes.<sup>6</sup>  $S = 0.5$  at characteristic radius  $r = 4r_{\text{in}}$  where the dissipation  $4\pi H r^2 \dot{q}^+ \propto S/r$  peaks (see eq. [40] below). One expects rotating holes in GRBs, and  $r \approx 3r_g$  is reasonable. The accretion time is

$$t_a(r) = \frac{r}{u^r} = \frac{S}{\alpha \Omega_K} \left(\frac{H}{r}\right)^{-2} = 2.9 \times 10^{-3} S \left(\frac{2H}{r}\right)^{-2} \left(\frac{\alpha}{0.1}\right)^{-1} \left(\frac{r}{3r_g}\right)^{3/2} \left(\frac{M}{M_\odot}\right) \text{ s.} \quad (37)$$

We neglect here the disk gravity, which is a valid approximation as long as  $\dot{M} t_a \ll M$ , where  $\dot{M}$  is the accretion rate. The typical  $t_a$  is much shorter than the burst duration, and accretion is viewed as a quasi-steady process. It can power a relativistic outflow (“fireball”) with luminosity

$$L = \epsilon_f \dot{M} c^2 \approx 10^{51} \left(\frac{\epsilon_f}{0.01}\right) \left(\frac{\dot{M}}{10^{32} \text{ g s}^{-1}}\right) \text{ erg s}^{-1}, \quad (38)$$

where  $\epsilon_f$  is the efficiency of  $\dot{M}c^2$  conversion into a fireball. A likely  $\epsilon_f$  is below the net efficiency  $\epsilon \sim 0.1$  of accretion: most of the energy is either carried away by neutrinos or advected by the accretion flow (in case of small neutrino losses).

The disk baryonic density is given by

$$\rho = \frac{\dot{M} t_a}{4\pi r^2 H} \approx 6.6 \times 10^{10} S \left(\frac{2H}{r}\right)^{-3} \left(\frac{r}{3r_g}\right)^{-3/2} \left(\frac{\alpha}{0.1}\right)^{-1} \left(\frac{M}{M_\odot}\right)^{-2} \left(\frac{\dot{M}}{10^{32}}\right) \text{ g cm}^{-3}, \quad (39)$$

and it is heated viscously with rate

$$\dot{q}^+ = \frac{3\dot{M}\Omega_K^2}{8\pi H} S \approx 5.2 \times 10^{33} S \left(\frac{2H}{r}\right)^{-1} \left(\frac{r}{3r_g}\right)^{-4} \left(\frac{\dot{M}}{10^{32}}\right) \left(\frac{M}{M_\odot}\right)^{-3} \text{ erg cm}^{-3} \text{ s}^{-1}. \quad (40)$$

The flow has a huge optical depth for photons, and radiation diffusion is negligible on the accretion timescale. The only cooling mechanism is neutrino emission, which becomes efficient at  $\dot{M} \gtrsim 10^{31} \text{ g s}^{-1}$  and small  $r$  (e.g. Popham, Woosley, & Fryer 1999; Narayan, Piran, & Kumar 2001;

---

<sup>6</sup>We give here simple Newtonian estimates and trace the hole spin only through its effect on  $r_{\text{in}}$ ; other relativistic corrections are modest and weakly affect the results.

Kohri & Mineshige 2002). An upper bound on temperature is derived from assumption that the flow does not loose the dissipated energy and instead traps it and advects. The advective flow has energy density  $w \approx \dot{q}^+ t_a \approx (3/8)(r_g/r)\rho c^2$  (we use eqs. [37] and [40] with  $S = 0.5$ ). The energy density in such a hot flow is dominated by radiation and  $e^\pm$ , so that

$$\frac{11}{4}aT_{\max}^4 \approx \frac{3r_g}{8r}\rho c^2, \quad (41)$$

where  $11/4$  accounts for the contribution of relativistic weakly degenerate  $e^\pm$ . Neutrinos make a noticeable contribution to the energy density if they are thermalized, and then  $T_{\max}$  will be slightly lower. Equation (41) yields

$$kT_{\max} \approx 13 \left( \frac{\rho}{10^{11}} \right)^{1/4} \left( \frac{r}{3r_g} \right)^{-1/4} \text{ MeV.} \quad (42)$$

The actual temperature can be significantly lower because of neutrino cooling. The main cooling process is  $e^\pm$  capture on nucleons (the Urca process):  $e^- + p \rightarrow n + \nu$  and  $e^+ + n \rightarrow p + \bar{\nu}$ , which also shapes  $Y_e$  as we discussed in § 2.1. We now evaluate the minimum accretion rate  $\dot{M}_{\text{eq}}$  above which the Urca process is rapid enough to establish an equilibrium  $Y_e$ . The equilibrium is achieved when the flow has emitted one neutrino per nucleon.

It is easy to see that  $\nu$ -cooled disks must reach the equilibrium  $Y_e$ . Indeed, the mean energy of the emitted neutrinos,  $\lesssim 30$  MeV, is below the liberated accretion energy per nucleon,  $\sim 100–300$  MeV, and the efficient cooling implies that more than one neutrino per nucleon is produced. Thus,  $\dot{M}_{\text{eq}}$  should be looked for in the inefficient (advective) regime with  $T \approx T_{\max}$ . Such a flow is only mildly degenerate, and the rates of  $e^\pm$  capture read in the zero order in  $\mu/\theta$ ,

$$\dot{n}_{e^-p} \approx 1.5 \times 10^{-2} n_p \theta^5, \quad \dot{n}_{e^+n} \approx 1.5 \times 10^{-2} n_n \theta^5. \quad (43)$$

The neutronization timescale is  $t_n = n_p/\dot{n}_{e^-p} \approx 70\theta^{-5}$  s, and it should be compared with the accretion timescale  $t_a$  (eq. 37),

$$\frac{t_n}{t_a} \approx 70 \frac{\alpha \Omega_K}{S \theta_{\max}^5} \left( \frac{H}{r} \right)^2. \quad (44)$$

We take into account the hydrostatic balance  $(H/r)^2 \approx (aT_{\max}^4/\rho c^2)(2r/r_g) = 3/11$ , and use equation (39) with  $S = 0.5$  to get

$$\frac{t_n}{t_a} \approx 2 \times 10^{-2} \left( \frac{r}{3r_g} \right)^{13/8} \left( \frac{\alpha}{0.1} \right)^{9/4} \left( \frac{M}{M_\odot} \right)^{3/2} \left( \frac{\dot{M}}{10^{32}} \right)^{-5/4}. \quad (45)$$

We conclude that disks with

$$\dot{M} > \dot{M}_{\text{eq}} \approx 10^{31} \left( \frac{r}{3r_g} \right)^{13/10} \left( \frac{\alpha}{0.1} \right)^{9/5} \left( \frac{M}{M_\odot} \right)^{6/5} \text{ g s}^{-1} \quad (46)$$

achieve the equilibrium  $Y_e$ . This range covers plausible  $\dot{M}$  for GRBs.

The equilibrium  $Y_e < 0.5$  if the flow temperature is below the neutronization temperature  $T_n$  that was calculated in § 2.1 (eqs. [14] and [23]). It is instructive to compare  $T_n$  with the maximum temperature  $T_{\max}$  (eq. 41),

$$\frac{T_n}{T_{\max}} \approx \kappa \left( \frac{\rho}{10^{11}} \right)^{1/4} \left( \frac{r}{3r_g} \right)^{1/4}, \quad (47)$$

where  $\kappa = 2.5$  for  $\nu$ -transparent and  $\kappa = 1.5$  for  $\nu$ -opaque flows. The neutron-excess condition  $T < T_n$  is most difficult to satisfy in low- $\dot{M}$  flows, when the neutrino cooling is inefficient and  $T \approx T_{\max}$ . Such flows are  $\nu$ -transparent, so that  $\kappa = 2.5$  should be used in equation (47). Substituting equation (39),  $T = T_{\max}$ , and  $(H/r)^2 = 3/11$ , we find that  $T_{\max} < T_n$  if

$$\dot{M} > \dot{M}_n \approx 10^{31} \left( \frac{r}{3r_g} \right)^{3/2} \left( \frac{\alpha}{0.1} \right) \left( \frac{M}{M_{\odot}} \right)^2 \text{ g s}^{-1}. \quad (48)$$

The “neutronization” accretion rate  $\dot{M}_n$  is comparable to  $\dot{M}_{\text{eq}}$ . Plausible  $\dot{M}$  in GRB accretion flows are  $10^{32}$  g/s and higher, and they should have a neutron excess.

### 2.3. De-neutronization in the fireball?

Are outflows from neutron-rich engines also neutron-rich? The fireball picks up baryons from the surface of the central engine, and the surface density is relatively low. The matter might change  $Y_e$  while escaping.

Let us consider fireballs from accretion disks. The disk is turbulent (the turbulence is the source of viscosity that is responsible for accretion), and it is mixed in the vertical direction on the sound-crossing timescale  $t_{\text{mix}} \approx H/c_s$  (the turbulent velocity is slightly smaller than  $c_s$ , however, the thickness of surface layers is also smaller than  $H$ , and  $t_{\text{mix}} \approx H/c_s$  is about right). Given the hydrostatic balance,  $H = c_s/\Omega_K$ , one gets

$$t_{\text{mix}} \approx \Omega_K^{-1}. \quad (49)$$

The escape timescale of the fireball also approximately equals  $\Omega_K^{-1}$ . The turbulent material circulates rapidly up to the surface and back to the interior of the disk, and a small portion of it can be (also rapidly) lost in each circulation. As an element of matter elevates to the surface and expands, its  $Y_e$  would increase if it adjusted instantaneously to the new equilibrium value. However, the time the element has before it sinks back or escapes,  $\Omega_K^{-1}$ , can be too short for the adjustment. Then  $Y_e$  of the escaping matter corresponds to  $\rho$  and  $T$  *inside* the disk, where it has spent almost all the time before the sudden escape.

To check this picture, let us evaluate the timescale of “de-neutronization” of an initially neutron rich material that has suddenly expanded into a low-density, hot fireball. Neutrons tend to convert back into protons via two charged current reactions:  $e^+$  capture and  $\nu$  absorption ( $\beta$ -decay is

slow and negligible). The fireball has temperature  $\theta > 1$  and non-degenerate electrons  $\mu \ll \theta$ . Equation (43) gives the  $e^+$  capture timescale

$$t_+ = \frac{n_n}{\dot{n}_{e^+n}} \approx \frac{70}{\theta^5} \text{ s}, \quad (50)$$

$$t_+ \Omega_K = 1.4 \times 10^2 \left( \frac{kT}{3 \text{ MeV}} \right)^{-5} \left( \frac{r}{3r_g} \right)^{-3/2} \left( \frac{M}{M_\odot} \right)^{-1}. \quad (51)$$

For fireball temperatures up to 8 MeV, the  $e^+$ -capture is slow compared to  $\Omega_K^{-1}$ , and it does not affect  $Y_e$  of the escaping material.

The cross section of neutrino absorption by nucleon is

$$\sigma_\nu = 1.4 \times 10^{-44} [1 - f_-(\omega + Q)] (\omega + Q)^2 \left[ 1 - \frac{1}{(\omega + Q)^2} \right]^{1/2} \text{ cm}^2 \approx 1.4 \times 10^{-44} \omega^2 \text{ cm}^2, \quad (52)$$

and the corresponding rate of de-neutronization is

$$\dot{n}_n = cn_n \int_0^\infty n_\omega \sigma_\nu d\omega, \quad (53)$$

where  $n_\omega = dn_\nu/d\omega$  is the spectrum of the neutrino number density. This gives the timescale of de-neutronization,

$$t_\nu = \frac{n_n}{\dot{n}_n} = \frac{2.4 \times 10^{33}}{\bar{n}_n \bar{\omega}^2} \text{ s}, \quad (54)$$

where bar denotes averaging over the neutrino spectrum. A maximum neutrino density outside the disk is given by

$$n_\nu \approx \frac{3\dot{M}\Omega_K^2 S}{8\bar{\omega}m_e c^3}, \quad (55)$$

which assumes that the neutrino energy flux  $F_\nu \approx n_\nu \bar{\omega} m_e c^3 / \pi$  equals the flux of the released accretion energy,  $F = (3/8\pi)GMM\dot{S}/r^3$ . For the maximum  $n_\nu$ , we get

$$t_\nu \Omega_K \approx \frac{10^2}{S} \frac{\bar{\omega}}{\bar{\omega}^2} \left( \frac{\dot{M}}{10^{32}} \right)^{-1} \left( \frac{M}{M_\odot} \right) \left( \frac{r}{3r_g} \right)^{3/2}. \quad (56)$$

The mean  $\omega$  and  $\omega^2$  are determined by the state of the material that emits neutrinos. If the disk is  $\nu$ -transparent, the neutrions have the spectrum

$$n_\omega \propto (\omega + Q)^2 \left[ \exp \left( \frac{\omega + Q - \mu}{\theta} \right) + 1 \right]^{-1} \left[ 1 - \frac{1}{(\omega + Q)^2} \right]^{1/2} \omega^2 \approx \omega^4 \left[ \exp \left( \frac{\omega}{\theta} \right) + 1 \right]^{-1}, \quad (57)$$

where  $\theta$  is temperature inside the disk, and  $Q$  and  $\mu$  have been neglected compared to the typical  $\omega = \bar{\omega}$ . This gives  $\bar{\omega} \approx 5\theta$  and  $\bar{\omega}^2 \approx 23\theta^2$ . The optical depth of the disk for neutrino absorption by nucleons is

$$\tau_\nu \approx 0.1 \left( \frac{T}{T_{\max}} \right)^{-5} \left( \frac{r}{3r_g} \right)^{-7/4} \left( \frac{\alpha}{0.1} \right)^{-3/2} \left( \frac{M}{M_\odot} \right)^{-2} \left( \frac{\dot{M}}{10^{32}} \right)^{3/2}. \quad (58)$$

From equations (56) and (58) one can see that  $\nu$ -transparent disks typically have  $t_\nu \Omega_K > 1$ , and hence their fireballs should not be de-neutronized.

The high- $\dot{M}$  (and  $\nu$ -opaque) disks produce sufficiently high neutrino fluxes that can impact  $Y_e$  of the ejected fireball. In this case, the neutrinos have a blackbody spectrum with  $\bar{\omega} \approx 3.1\theta_\nu$  and  $\bar{\omega}^2 \approx 12\theta_\nu^2$ , where  $\theta_\nu$  is the temperature of the  $\nu$ -photosphere. The disk also emits  $\bar{\nu}$  from a corresponding  $\bar{\nu}$ -photosphere. Both  $\nu$  and  $\bar{\nu}$  absorptions occur in the fireball and set a new equilibrium  $Y_e$  such that the rates of  $\nu$  and  $\bar{\nu}$  absorptions are equal. The new  $Y_e$  should be below 0.5 (see Qian et al. 1993 where a similar problem is discussed in the context of supernova engines). This expectation is based on two facts: (1) the number densities of  $\nu$  and  $\bar{\nu}$  are approximately equal,  $|n_\nu - n_{\bar{\nu}}| \ll n_\nu$ , — otherwise they carry away a too large leptonic number from the disk, and (2) the absorption cross section is proportional to the neutrino energy squared. It gives the equilibrium n/p-ratio,  $n_n/n_p \approx \theta_{\bar{\nu}}^2/\theta_\nu^2 > 1$ , where  $\theta_\nu$  and  $\theta_{\bar{\nu}}$  are the temperatures of the  $\nu$  and  $\bar{\nu}$  photospheres. The  $\bar{\nu}$  temperature is higher because the neutronized disk is more transparent for  $\bar{\nu}$ , so that the  $\bar{\nu}$ -photosphere is deeper in the disk and hotter.

### 3. Nucleosynthesis

When the temperature of the expanding fireball decreases to  $\sim 100$  keV, fusion reactions shape the nuclear composition like they do during the primordial nucleosynthesis in the Universe (Wagoner, Fowler, & Hoyle 1967). In both cases, we deal with an expanding blackbody fireball with initially free nucleons, and the following three parameters control the outcome of nucleosynthesis: (1) photon-to-baryon ratio  $\phi = n_\gamma/n_b$ , (2) the expansion timescale  $\tau_*$  at the time of nucleosynthesis, and (3) the n/p-ratio prior to the onset of nucleosynthesis. In the Universe,  $\phi \approx 3 \times 10^9$ ,  $\tau_* \approx 10^2$  s, and  $n_n/n_p \approx 1/7$ . Below we formulate the nucleosynthesis problem in GRBs and give a qualitative comparison of the problem with the big bang. Then we perform detailed calculations of the nuclear reactions in GRB ejecta.

#### 3.1. Ejecta model

Let us consider a central engine that ejects baryonic matter at a rate  $\dot{M}_b$  [g/s] and thermal energy at a rate  $L_{\text{th}} \gg \dot{M}_b c^2$ . The fireball is likely to carry magnetic fields, and the corresponding Poynting luminosity  $L_P$  may be much higher than the thermalized luminosity. The magnetic fields then prolong the fireball acceleration at late stages, after all the thermal energy has been converted into bulk expansion. The maximum Lorentz factor of the fireball can be estimated as  $\Gamma_{\text{max}} = (L_{\text{th}} + L_P)/\dot{M}_b c^2$ , which is at least  $10^2$  for GRB explosions.

Nucleosynthesis occurs when the fireball temperature drops to about  $kT_* \sim 100$  keV at a radius  $R_* \sim 10^7 - 10^9$  cm. The timescale of expansion to this radius,  $R_*/c$ , is much smaller than the duration of the central engine activity. Therefore, in the nucleosynthesis calculations, the fireball

can be modeled as a quasi-steady outflow. Let us assume that it expands in an axisymmetric funnel with spherical cross section

$$S(R) = S_0 \left( \frac{R}{r_0} \right)^\psi. \quad (59)$$

For example,  $\psi = 2$  for a radial funnel (and also for a spherically symmetric explosion), and  $\psi = 1$  for a parabolic funnel that may develop in a collapsing progenitor of the GRB (Mészáros & Rees 2001). The outflow is a relativistic ideal fluid with baryon density  $\rho$ , pressure  $P$  and energy density  $w = 3P \gg \rho c^2$ ; all these magnitudes are measured in the fluid rest frame. In spherical coordinates  $x^i = (t, R, \theta, \phi)$ , the outflow has 4-velocity  $u^i = dx^i/d\tau = (u^t, u^R, u^\theta, u^\phi)$ , where  $\tau$  is proper time. We assume  $u^\phi = 0$  and  $Ru^\theta \ll u^t, u^R$ . The latter assumption is satisfied at all radii for a radial explosion ( $u^\theta = 0$ ) and at  $R \gg r_0$  for a collimated explosion ( $\psi < 2$ ).

The outflow dynamics is governed by the conservation laws  $\nabla_i(\rho u^i) = 0$  and  $\nabla_i(T_k^i) = 0$ , where  $T_k^i = u^i u_k (w + P) + P \delta_k^i$  is the stress-energy tensor. The electromagnetic tensor is not included here, which greatly simplifies the problem (we are interested in the early hot stage when the expansion is likely driven by thermal pressure even in the presence of strong fields). Then the baryon and energy conservation laws read

$$S\rho u^R = \dot{M}_b, \quad S(w + P)u^t u^R = L_{\text{th}}. \quad (60)$$

The high Lorentz factor of the expansion,  $\Gamma \gg 1$ , implies  $u^R/c \approx u^t = \Gamma$ . Equations (60) then yield

$$\rho = \frac{\dot{M}_b}{S\Gamma c}, \quad \frac{w}{\rho} = \frac{3}{4} \frac{L_{\text{th}}}{\dot{M}_b \Gamma}. \quad (61)$$

We assume that the outflow does not exchange mass or energy with the surroundings, i.e.,  $\dot{M}_b(R) = \text{const}$  and  $L_{\text{th}}(R) = \text{const}$ . Equation (61) then gives  $w \propto \rho/\Gamma$  while the first law of thermodynamics  $d(w/\rho) = -Pd(1/\rho)$  gives  $w \propto \rho^{4/3}$ . Excluding  $\rho$  from these two relations, one gets  $w^{1/4} \propto 1/\Gamma$  and

$$T\Gamma = T_0, \quad (62)$$

where  $T_0$  is a constant. Equation (62) is strictly valid at temperatures  $kT \ll m_e c^2 = 511$  keV where the  $e^\pm$  energy density can be neglected. At small  $\Gamma$  (where  $kT \gtrsim m_e c^2$ ), the inclusion of  $e^\pm$  reduces  $T$  by a modest factor  $(11/4)^{-1/4}$ .

Equation (60) implies  $w = aT^4 \propto (\Gamma^2 S)^{-1}$ , and, combining with equation (62), one gets

$$\Gamma = \frac{T_0}{T} = \left( \frac{S}{S_0} \right)^{1/2} = \left( \frac{R}{r_0} \right)^{\psi/2}. \quad (63)$$

The outflow may be collimated already at the base into a solid angle  $\Omega_0 = S_0/r_0^2 < 4\pi$ . Its transonic dynamics near the engine is complicated and unknown. With a reasonable accuracy, the simple estimate  $L_{\text{th}} \approx S_0 a T_0^4 c$  gives

$$kT_0 \approx 2 \left( \frac{L_{\text{th}}}{10^{51}} \right)^{1/4} \left( \frac{r_0}{3 \times 10^6} \right)^{-1/2} \left( \frac{\Omega_0}{4\pi} \right)^{-1/4} \text{ MeV.} \quad (64)$$

The value of  $T_0$  is most sensitive to the engine size  $r_0$ . It can be as small as  $3 \times 10^5$  cm (if the outflow is powered by a Kerr black hole via the Blandford-Znajek process) or as large as  $10^7$  cm (if the outflow is powered by an accretion disk).

An important parameter of the nucleosynthesis problem is the photon-to-baryon ratio  $n_\gamma/n_b = (w/2.7kT)(\rho/m_p)^{-1}$ . It is constant, and its value is found from equations (61,62),

$$\phi = \frac{n_\gamma}{n_b} = \frac{3}{4} \frac{\eta_{\text{th}} m_p c^2}{2.7 k T_0} = 7.7 \times 10^4 \left( \frac{k T_0}{1 \text{ MeV}} \right)^{-1} \left( \frac{\eta_{\text{th}}}{300} \right), \quad \eta_{\text{th}} = \frac{L_{\text{th}}}{\dot{M} c^2}. \quad (65)$$

The typical  $\phi$  is 5 orders of magnitude smaller compared to that of the Universe.

Nucleosynthesis must occur during the acceleration stage of the fireball because the acceleration ends at a very low temperature  $T = T_0/\Gamma_{\text{max}} \ll T_*$ . The accelerated expansion is described in comoving time by  $d\tau = dt/\Gamma \approx dR/c\Gamma$ , which gives (we make use of eq. 63)

$$\tau(T) = \begin{cases} \frac{r_0}{c} \log \left( \frac{T_0}{T} \right) & \psi = 2, \\ \frac{r_0}{c} \frac{2}{(2-\psi)} \left( \frac{T}{T_0} \right)^{(\psi-2)/\psi} & \psi < 2. \end{cases} \quad (66)$$

The expansion timescale at the time of nucleosynthesis,  $\tau_* = \tau(R_*)$ , depends on the shape of the funnel;  $\tau_* \approx 3r_0/c$  for  $\psi = 2$  and  $\tau_* \approx 2(T_0/T_*)(r_0/c)$  for  $\psi = 1$ .

Note that  $L_{\text{th}}$ ,  $\dot{M}$ , and  $T_0$  enter the nucleosynthesis problem only in combinations that determine  $\phi$  and  $\tau(T)$ , and play no other role. For example, the initial temperature is not important as long as  $kT_0 > 200$  keV.

### 3.2. Simple estimates and comparison to the big bang

First we evaluate the temperature  $T_*$  at which we expect the nucleosynthesis to begin. Let us remind why  $kT_* \approx 80$  keV in the big bang. If the nuclear statistical equilibrium (NSE) were maintained, recombination of nucleons into  $\alpha$ -particles would occur at  $kT \sim 200$  keV (e.g. Meyer 1994). The reason of the nucleosynthesis delay until  $kT \approx 80$  keV is what is sometimes called “deuterium bottleneck”. Before fusing into  $\alpha$ -particles, the nucleons have to form lighter nuclei: deuterium, tritium, or  $^3\text{He}$ . At  $kT > 100$  keV, the equilibrium abundances of these elements are very low, which implies a very long timescale for fusion, and helium is not formed even though it is favored by the NSE. In particular, the deuterium abundance is suppressed by the very fast photodisintegration  $\gamma + d \rightarrow n + p$  that balances the opposite reaction  $n + p \rightarrow d + \gamma$  at (e.g. Esmailzadeh, Starkman, & Dimopoulos 1991)

$$Y_d \approx 7 \times 10^{-6} \phi^{-1} Y_n Y_p T_9^{3/2} \exp \left( \frac{25.8}{T_9} \right). \quad (67)$$

Here  $Y_i = n_i/n_b$  is abundance of the  $i$ -th element and  $T_9 = T/10^9 \text{ K} = kT/86.17$  keV. Nucleosynthesis starts when the exponential wins the pre-exponential factor to give a noticeable  $Y_d \sim 10^{-3}$ . Substituting  $\phi = 3 \times 10^9$ , one finds that it happens at  $kT_* \approx 80$  keV.

In GRB outflows,  $\phi$  is 5 orders of magnitude smaller, and the NSE recombination would happen at  $kT \sim 500$  keV. The actual nucleosynthesis temperature  $T_*$  is also higher compared to the big bang — it depends logarithmically on  $\phi$ . Using equation (67), we find  $kT_* \approx 140$  keV for GRBs.

At a given  $T$ , nuclear reaction rates scale as  $\dot{Y} \propto \rho \propto \phi^{-1}$  (here  $Y$  is an element abundance). The ratio of a reaction timescale,  $\tau_{\text{reac}} = Y/\dot{Y}$ , to the expansion rate,  $Y/\tau$ , behaves as  $\phi/\tau$ . This combination is  $\sim 3 - 30$  times smaller in GRBs compared to the big bang nucleosynthesis, which may seem not a crucial difference. In fact, even the big bang was dangerously close to the freezeout of the neutron capture reaction  $n + p \rightarrow d + \gamma$ , without which nucleosynthesis cannot start. It is therefore instructive to compare the capture timescale with the expansion timescale in GRBs.

The neutron capture rate varies slowly with temperature (see Fig. 11 in Smith, Kawano, & Malaney 1993), and near 100 keV it is approximately  $\dot{Y}_c \approx 2.5 \times 10^4 \rho Y_p Y_n$ . The reaction timescale is

$$\tau_c = \frac{\min\{Y_p, Y_n\}}{\dot{Y}_c} = \frac{1.2 \times 10^{-9} \phi}{T_9^3 \max\{Y_n, Y_p\}}. \quad (68)$$

It should be compared to the time  $\tau_*$  it takes the fireball to expand by a factor of two at the epoch of nucleosynthesis. For the big bang,  $\tau_*/\tau_c \sim 30$ . For GRBs, we get

$$\tau_c \approx 10^{-4} \left( \frac{\phi}{10^5} \right) \left( \frac{Y_n}{0.5} \right)^{-1} \text{ s}, \quad (69)$$

$$\frac{\tau_*}{\tau_c} \approx \begin{cases} \left( \frac{\phi}{10^5} \right)^{-1} \left( \frac{r_0}{3 \times 10^6} \right) \left( \frac{Y_n}{0.5} \right) & \psi = 2, \\ \left( \frac{\phi}{10^5} \right)^{-1} \left( \frac{r_0}{3 \times 10^6} \right) \left( \frac{Y_n}{0.5} \right) \left( \frac{T_0}{T_*} \right) & \psi = 1. \end{cases} \quad (70)$$

One can see that, in a radial explosion ( $\psi = 2$ ), the neutron capture rate is marginal for successful helium production. In a collimated explosion, the ratio  $\tau_*/\tau_c$  is higher by a factor of  $T_0/T_* \sim 10$ , and the nucleosynthesis is more efficient.

An important difference between the GRBs and the big bang is the n/p-ratio. In the big bang,  $n_n/n_p = 1/7$  ( $Y_e = 7/8$ ), which leads to 25% mass fraction of helium after the n-p recombination, while 75% of mass remains in protons (and a tiny amount of other nuclei). In GRBs,  $n_n/n_p > 1$  ( $Y_e < 0.5$ ), and there are leftover neutrons even if all protons are consumed by helium production. The minimum mass fraction of leftover neutrons is

$$X_n = 1 - 2Y_e. \quad (71)$$

### 3.3. Detailed calculation

#### 3.3.1. The code

We will keep track of elements with mass numbers less than 4 (like the big bang nucleosynthesis, the abundances of heavier nuclei are very small). The six elements under consideration are n, p,

$^2\text{H}$ ,  $^3\text{H}$ ,  $^3\text{He}$ , and  $^4\text{He}$ ; they are denoted by  $n, p, d, t, 3, \alpha$ , respectively, and the photons are denoted by  $\gamma$ . Their abundances are measured by  $Y_i = n_i/n_b$  or  $X_i = A_i Y_i$ , where  $n_i$  and  $A_i$  are the number density and the mass number of the  $i$ -th nuclei. The photon and matter density are known functions of temperature,

$$n_\gamma = \frac{2}{\pi^2} \zeta(3) \left( \frac{kT}{\hbar c} \right)^3 = 2.0 \times 10^{28} T_9^3 \text{ cm}^{-3}, \quad \rho = 3.4 \times 10^4 \phi^{-1} T_9^3 \text{ g cm}^{-3}. \quad (72)$$

The evolution of nuclear composition is described by the set of equations

$$\dot{Y}_i = \Sigma Y_k Y_l [klij] - \Sigma Y_i Y_j [ijkl], \quad (73)$$

$$\dot{Y}_n = -\dot{Y}_d - 2\dot{Y}_t - \dot{Y}_3 - 2\dot{Y}_\alpha - \frac{Y_n}{\tau_\beta}, \quad (74)$$

$$\dot{Y}_p = -\dot{Y}_d - \dot{Y}_t - 2\dot{Y}_3 - 2\dot{Y}_\alpha + \frac{Y_n}{\tau_\beta}. \quad (75)$$

All the quantities here are measured in the matter rest frame:  $\tau_\beta = 890$  s is the mean lifetime of neutrons, the dot denotes the derivative with respect to the proper time  $\tau$ , and  $[ijkl] = n_b \bar{\sigma} v_{ij \rightarrow kl}$  is the rate of reaction  $i + j \rightarrow k + l$ . The sums in equation (73) are taken over all possible reactions with participation of the  $i$ -th nuclei. Not all reactions are important (Smith et al. 1993). For example, reactions that disrupt the  $\alpha$ -particles can be neglected as  $Y_\alpha$  is far below its equilibrium value. The included reactions are listed below.

Notice that it is sufficient to calculate the production and sink rates for deuterium, tritium, and helium isotopes  $^3\text{He}$  and  $^4\text{He}$  ( $i = d, t, 3, \alpha$  in eq. 73). Then  $\dot{Y}_n$  and  $\dot{Y}_p$  are found from the neutron and proton conservation laws (eqs. [74] and [75]), which include the  $Y_n/\tau_\beta$  term — the conversion of neutrons into protons via  $\beta$ -decay. The decay is negligible in GRBs, and we keep it for the code tests on big bang nucleosynthesis.

We include the following reactions in the calculations:  $n + p \leftrightarrow d + \gamma$ ,  $n + 3 \leftrightarrow p + t$ ,  $n + 3 \rightarrow \alpha + \gamma$ ,  $p + d \rightarrow 3 + \gamma$ ,  $p + t \rightarrow \alpha + \gamma$ ,  $d + d \rightarrow p + t$ ,  $d + d \rightarrow n + 3$ ,  $d + t \rightarrow n + \alpha$ ,  $d + 3 \rightarrow p + \alpha$ , and take their rates from Smith et al. (1993) and Esmailzadeh et al. (1991). We then have

$$\begin{aligned} \dot{Y}_d = & Y_n Y_p [npd\gamma] - Y_d Y_\gamma [d\gamma np] - Y_p Y_d [pd3\gamma] - 2Y_d^2 [ddn3] - Y_d Y_3 [d3p\alpha] \\ & - Y_d Y_t [dt\alpha] - 2Y_d^2 [ddpt], \end{aligned} \quad (76)$$

$$\dot{Y}_t = Y_d^2 [ddpt] + Y_n Y_3 [n3pt] - Y_d Y_t [dt\alpha] - Y_p Y_t [ptn3] - Y_p Y_t [pt\alpha\gamma], \quad (77)$$

$$\dot{Y}_3 = Y_p Y_d [pd3\gamma] + Y_d^2 [ddn3] + Y_p Y_t [ptn3] - Y_d Y_3 [d3p\alpha] - Y_n Y_3 ([n3pt] + [n3\alpha\gamma]), \quad (78)$$

$$\dot{Y}_\alpha = Y_d Y_t [dt\alpha] + Y_d Y_3 [d3p\alpha] + Y_n Y_3 [n3\alpha\gamma] + Y_p Y_t [pt\alpha\gamma]. \quad (79)$$

The reaction rates are functions of  $T$  and  $\rho$ , and the set of equations is closed by equation (66) that relates  $T$  and  $\tau$ . We solve equations (74-79) numerically with initial conditions  $Y_p^0 = Y_e$ ,  $Y_n^0 = 1 - Y_e$ ,  $Y_\alpha = 0$ , and  $\dot{Y}_d = \dot{Y}_t = \dot{Y}_3 = 0$  at an initial temperature  $kT_0 \sim 1$  MeV. At high temperatures, the abundances of all elements except  $n$  and  $p$  are negligibly small. The abundances

of deuterium, tritium, and  $^3\text{He}$  are close to quasi-steady equilibrium (QSE) at all  $kT > 150$  keV, i.e. their production  $\dot{Y}^+$  and destruction  $\dot{Y}^-$  rates are much higher than the expansion rate  $Y/\tau$ , and hence  $\dot{Y}^+$  and  $\dot{Y}^-$  almost balance each other. Near the QSE, an element abundance  $Y$  is determined by setting the net  $\dot{Y} = \dot{Y}^+ - \dot{Y}^- = 0$ . (Thus, one avoids numerical integration where  $\dot{Y}$  is a small difference of big numbers.) The code has been tested with the big bang nucleosynthesis problem. It successfully reproduced the standard evolution of the cosmological nuclear composition.

### 3.3.2. Results

In Figure 3 we compare the GRB nucleosynthesis with that in the big bang. For the GRB explosion, we choose  $\phi = 10^5$ ,  $r_0 = 3 \times 10^6$  s,  $\psi = 2$ , and  $Y_e = 0.5$ . As expected, nucleosynthesis in GRBs occurs at higher temperatures, between 150 and 100 keV. The freezeout helium abundance turns out to be about 10%, and 90% of mass remains in free nucleons. Interestingly, the deuterium evolution is qualitatively different in GRBs:  $X_d$  increases monotonically and freezes out at a few percent level, 2.5 orders higher than in the big bang (see also Pruet et al. 2002). The deuterium production in the big bang is slow at late stages because of a low neutron abundance, and it falls behind the deuterium burning rate; thus, the burning wins and deuterium is depleted. The GRBs have more neutrons and negligible  $\beta$ -decay. As a result, the deuterium production exceeds the burning rate. Beside, the freezeout happens quickly in the exponential expansion,  $T \propto \exp(\tau/\tau_0)$ , and  $X_d$  could not decrease much below 1% even if the neutron capture reaction were completely switched off at  $kT < 80$  keV.

The outflow mass is dominated by free nucleons and helium, and one would like to know how their ratio depends on the parameters of the explosion. Figures 4 and 5 show the helium-to-nucleon mass ratio  $f$  as a function of  $\phi$  and  $r_0$  for  $Y_e = 0.5$ . The results can be approximated by

$$f = \frac{X_\alpha}{X_p + X_n} = \begin{cases} 0.2 \left( \frac{\phi}{10^5} \right)^{-1.4} \left( \frac{r_0}{3 \times 10^6} \right)^{1.1} & \psi = 2, \\ 7.6 \left( \frac{\phi}{10^5} \right)^{-1} \left( \frac{r_0}{3 \times 10^6} \right) & \psi = 1. \end{cases} \quad (80)$$

This formula can be viewed as a power-law expansion of  $f(\phi, r_0)$  near  $r_0 = 3 \times 10^6$  cm and  $\phi = 10^5$ . It has a good accuracy even when  $t_0$  and  $\phi$  vary by 2 orders of magnitude (a maximum error of  $\lesssim 2$  is reached in the corners of Figs. 4 and 5).

The helium production is most efficient in  $Y_e = 0.5$  models, where  $X_n^0 = X_p^0$ . We also did calculations for explosions with a neutron excess. For example, in a radial explosion with  $Y_e = 0.25$ , the freezeout helium abundance is lower by a factor of 1.6 compared to the corresponding models with  $Y_e = 0.5$ . This reduction factor weakly depends on  $\phi$  and  $t_0$ : it varies between 1.4 and 1.8 for the range of parameters shown in Figures 4 and 5.

The outflow is dominated by free nucleons where  $f < 1$ . For example, for a radial explosion with  $Y_e = 0.5$  it requires  $\phi > 3.1 \times 10^4 (r_0/3 \times 10^6)^{0.8}$ . The typical GRB parameters happen to be

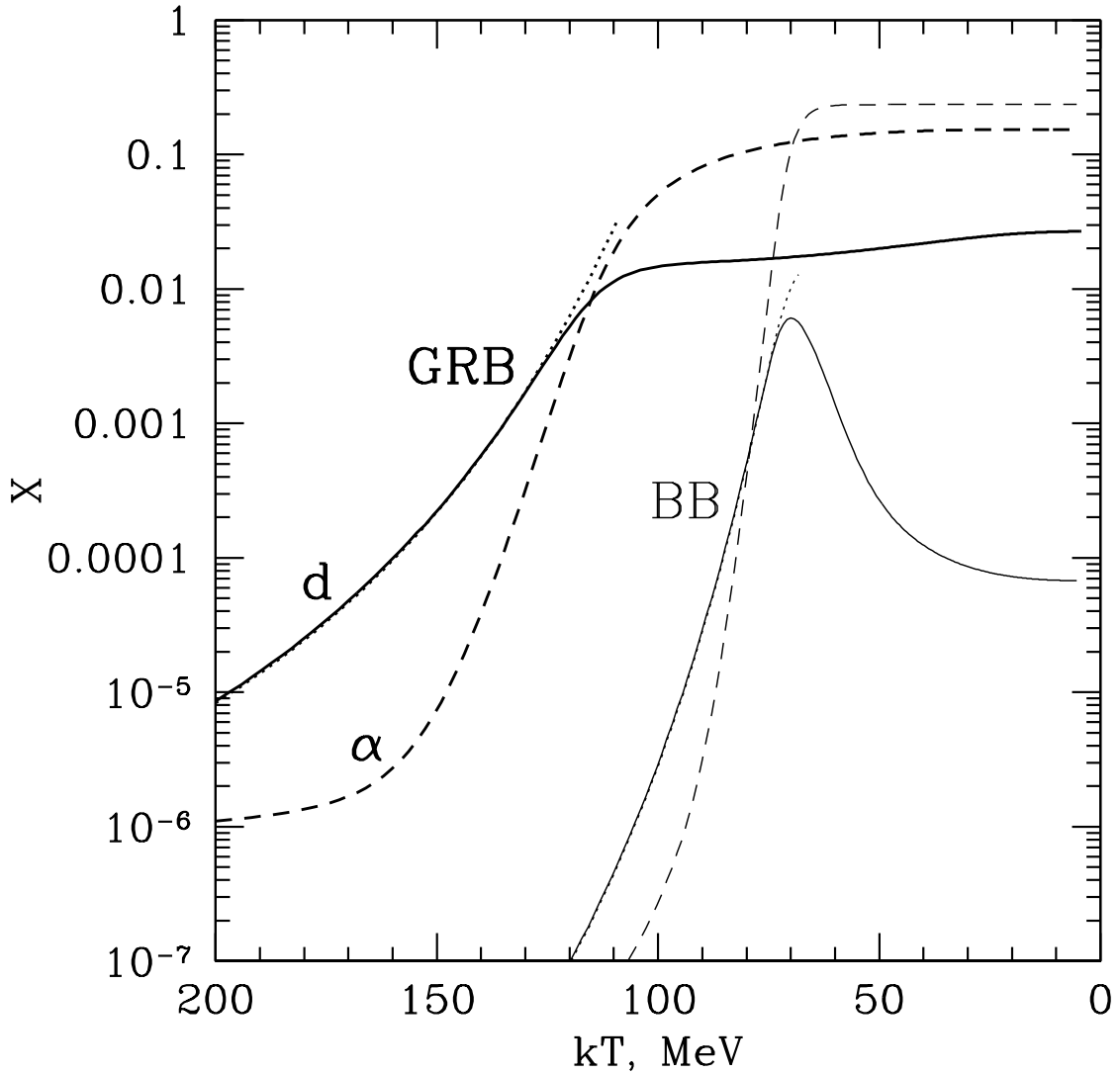


Fig. 3.— Evolution of deuterium and helium abundances with temperature in an expanding fireball. The (thicker) GRB curves are calculated for a radial explosion with  $\phi = n_\gamma/n_b = 10^5$  and  $r_0 = 3 \times 10^6$  cm. For comparison, the big bang (BB) nucleosynthesis is also shown (with  $\phi = 3 \times 10^9$ ). The dotted curves show the QSE (production=disruption) abundances of deuterium.

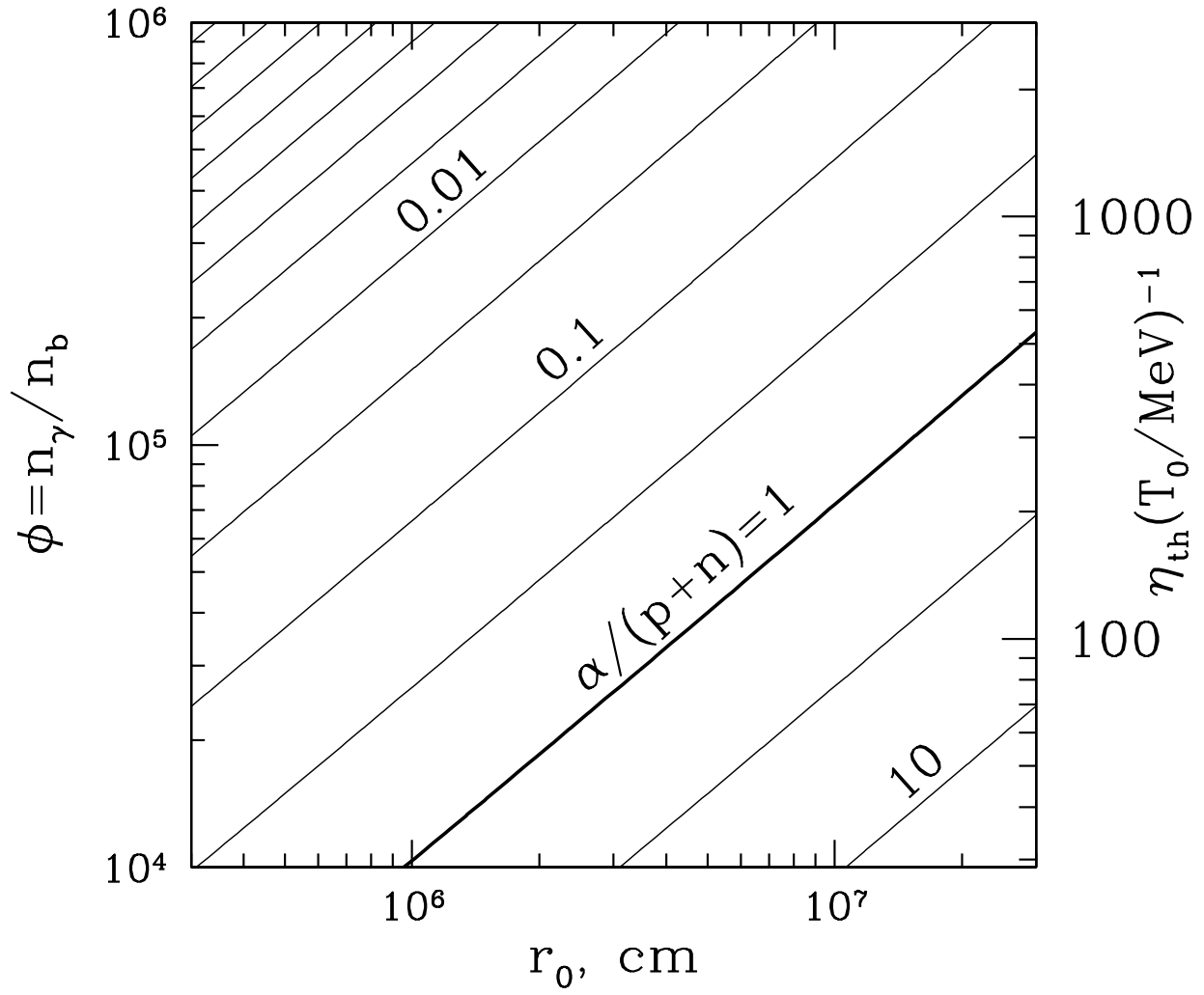


Fig. 4.— Contours of helium-to-nucleon ratio  $f(\phi, r_0) = \text{const}$  for radial explosions with  $Y_e = 0.5$ . Right axis shows  $(L_{\text{th}}/\dot{M}c^2)(kT_0/\text{MeV})^{-1}$  related to  $\phi$  by equation (65). If the fireball is not Poynting-flux dominated, its final Lorentz factor equals  $\eta_{\text{th}} = L_{\text{th}}/\dot{M}c^2$ .

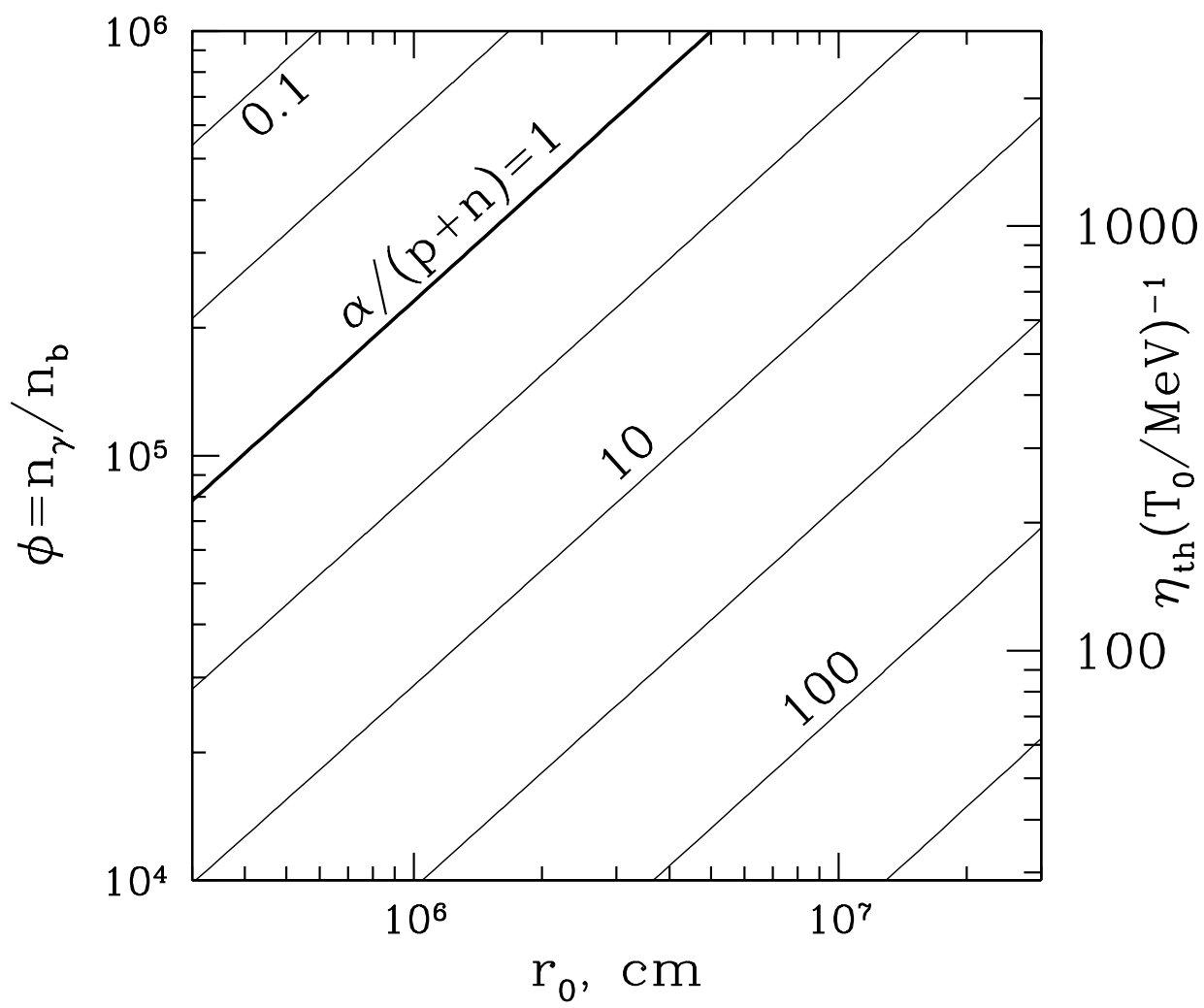


Fig. 5.— Same as in Figure 4 but for parabolically collimated explosions.

just marginal for successful nucleosynthesis:  $f$  varies from almost zero to ten in the expected range of  $\phi$  and  $r_0$ . Even under conditions most favorable for helium formation, leftover neutrons have a sizable mass fraction.

#### 4. Helium spallation

Synthesized helium may be disrupted during the subsequent evolution of the explosion. Spallation reactions can occur when an  $\alpha$ -particle collides with another particle with relative energy exceeding the nuclear binding energy. The temperature at the acceleration stage is too low for such reactions, however, the collisions may become energetic if (1) there appears a substantial relative bulk velocity between the neutron and ion components of the ejecta or (2) internal shocks occur and heat the ejecta to a high temperature.

##### 4.1. Neutron-ion collisions during the acceleration stage

Near the central engine, the neutron component of the fireball is well coupled to the ion component by elastic collisions with a small relative velocity  $\tilde{\beta} = \tilde{v}/c$  (Derishev et al. 1999, Bahcall & Mészáros 2000). The collision cross section can be approximated as  $\sigma_i = \sigma_0/\tilde{\beta}$ , where  $\sigma_0 \approx 3 \times 10^{-26} \text{ cm}^2$  if the ions are protons (and  $\sigma_0$  approaches  $10^{-25} \text{ cm}^2$  for  $\alpha$ -particles). In the fluid frame, the mean collisional time for neutrons is  $\tau_{\text{coll}} = (n_i \sigma_i \tilde{\beta} c)^{-1} = (n_i \sigma_0 c)^{-1}$ , where  $n_i$  is the ion density. The ions make a fraction of the baryon density  $n_b$ , which behaves as  $n_b = \text{const}/\Gamma^3$  during the acceleration stage. The constant of proportionality can be expressed in terms of  $\eta_{\text{th}} = L_{\text{th}}/\dot{M}c^2$  and  $\phi = n_\gamma/n_b$ ,

$$n_b = \frac{45^3 \zeta^4(3)}{4\pi^{14}} \left( \frac{m_p c}{\hbar} \right)^3 \frac{\eta_{\text{th}}^3}{\phi^4 \Gamma^3} = 5.61 \times 10^{38} \frac{\eta_{\text{th}}^3}{\phi^4 \Gamma^3}. \quad (81)$$

The ion fluid is accelerated by radiation or magnetic pressure, and its Lorentz factor grows by a factor of two on timescale  $t = R/c$ . The neutrons “miss” the ion acceleration by  $\Delta\Gamma/\Gamma \approx t_{\text{coll}}/t = \Gamma c \tau_{\text{coll}}/R < 1$  and have a smaller Lorentz factor  $\Gamma_n = \Gamma - \Delta\Gamma$ . The relative n-i velocity is  $\tilde{\beta} = (\Gamma^2 - \Gamma_n^2)/(\Gamma^2 + \Gamma_n^2) \approx (\Gamma - \Gamma_n)/\Gamma$ , which gives

$$\tilde{\beta} \approx \frac{t_{\text{coll}}}{t} \approx \frac{\Gamma}{R n_i \sigma_0} \propto \frac{\Gamma^4}{R}. \quad (82)$$

The energy of n-i collisions becomes sufficient for spallation reactions if  $\tilde{\beta}$  exceeds  $\tilde{\beta}_{\text{sp}} \approx 0.1$ . This can happen at late stages of the fireball acceleration, at high  $\Gamma$  but not exceeding the maximum  $\Gamma_{\text{max}} = L/\dot{M}c^2 = \eta_{\text{th}} + \eta_P$  ( $L = L_{\text{th}} + L_P$  is the total luminosity of the fireball that includes the Poynting flux). In the case of a radial explosion with  $\Gamma(R) \approx R/r_0$  we find that  $\tilde{\beta}$  reaches  $\tilde{\beta}_{\text{sp}}$  when  $\Gamma$  reaches

$$\Gamma_{\text{sp}} = 0.3 \Gamma_{\text{max}} \left( \frac{L_{\text{th}}}{L} \right) \left( \frac{\phi}{10^5} \right)^{-4/3} \left( \frac{\tilde{\beta}_{\text{sp}}}{0.1} \right)^{1/3} \left( \frac{r_0}{3 \times 10^6} \right)^{1/3} \left( \frac{n_i}{4n_b} \right)^{1/3}. \quad (83)$$

Spallation takes place if  $\Gamma_{\text{sp}} < \Gamma_{\text{max}}$ , which requires  $\phi > \phi_{\text{sp}}$ ,

$$\phi_{\text{sp}} \approx 4 \times 10^4 \left( \frac{L_{\text{th}}}{L} \right)^{3/4}. \quad (84)$$

We keep here  $L_{\text{th}}/L < 1$  as the most uncertain parameter, possibly much below unity. Note also, that in the case of a non-radial explosion,  $r_0$  should be replaced by  $R/\Gamma$  in equation (83). Using equation (65) it is easy to show that the condition  $\phi > \phi_{\text{sp}}$  is equivalent to

$$\Gamma_{\text{max}} > 160 \left( \frac{kT_0}{\text{MeV}} \right)^{1/3} \left( \frac{L}{L_{\text{th}}} \right)^{1/4}. \quad (85)$$

Let  $Y_n$  be abundance of neutrons that survived nucleosynthesis, and suppose that  $\phi > \phi_{\text{sp}}$ . The lifetime of  $\alpha$ -particles bombarded by the neutrons with  $\tilde{\beta} \approx \tilde{\beta}_{\text{sp}}$  is  $t_{\text{life}} \approx (t_{\text{coll}}/Y_n)(\sigma_0/\sigma_{\text{sp}}) \approx (\tilde{\beta}_{\text{sp}}/Y_n)t$ , where  $\sigma_{\text{sp}} \approx \sigma_0$  is the spallation cross section. A modest  $Y_n \sim 0.1$  is sufficient for significant spallation. Even a very small  $Y_n \ll 0.1$  might cause a runaway spallation process if the neutron yield is high enough in  $n - \alpha$  collisions; we did not investigate this possibility.

A complete neutron decoupling happens if  $\tilde{\beta}$  approaches unity. At this moment, the n-i collisions are energetic enough for pion production, which leads to multi-GeV neutrino emission (Derishev et al. 1999, Bahcall & Mészáros 2000). The corresponding Lorentz factor  $\Gamma$  is given by equation (83) with  $\tilde{\beta}_{\text{sp}}$  replaced by unity. The decoupling takes place if  $\phi$  exceeds

$$\phi_{\text{dec}} \approx 10^5 \left( \frac{L_{\text{th}}}{L} \right)^{3/4}. \quad (86)$$

The condition  $\phi > \phi_{\text{dec}}$  is equivalent to  $\Gamma_{\text{max}} > 400(kT_0/\text{MeV})(L/L_{\text{th}})^{1/4}$ . The decoupling is always preceded by spallation.

## 4.2. Internal shocks

The  $\alpha$ -particles can also be destroyed later on, when internal shocks develop in the ejecta. The Lorentz factor  $\Gamma_{\text{max}}$  fluctuates if the central engine is “noisy” during its operation  $0 < t < t_b \sim 1$  s. The fluctuations probably occur on timescales  $r_0/c \approx 10^{-4}$  s and longer, up to  $t_b$ . This leads to internal shocks (Rees & Mészáros 1994). Internal dissipation of the velocity fluctuations may give rise to the observed GRB, and this picture became popular because it easily accounts for the random short-timescale variations in the GRB light curves. The amplitude of the fluctuations is described by the dimensional rms of the Lorentz factor,  $A$ . At modest  $A \lesssim 1$ , the internal dissipation proceeds in a simple hierarchical manner (Beloborodov 2000). The internal collisions begin at

$$R_0 = \frac{2\Gamma_{\text{max}}^2}{A} \lambda_0 = 5.4 \times 10^{11} A^{-1} \left( \frac{\Gamma_{\text{max}}}{300} \right)^2 \left( \frac{\lambda_0}{3 \times 10^6} \right), \quad (87)$$

where  $\lambda_0$  is the minimum length scale of the fluctuations, which are probably comparable to  $r_0$ . The shortest fluctuations are dissipated first, and at  $R > R_0$  larger-scale fluctuations are dissipated in the hierarchical order.

#### 4.2.1. $n$ - $\alpha$ collisions

Suppose  $\Gamma_{\max}$  is small enough, so that the neutrons decouple from the ions after the acceleration stage and have same  $\Gamma = \Gamma_{\max}$ . As soon as caustics (shocks) develop in the ion component, the neutrons begin to drift with respect to the ions. Their relative velocity  $\tilde{\beta} \approx A$  is sufficient for spallation reactions if  $A > 0.1$  (and for  $A \sim 1$  the pion production and multi-GeV neutrino emission takes place, see Mészáros & Rees 2000).

Let  $dL/d\Omega = R^2 n_b m_p c^3 \Gamma^2$  be the fireball luminosity per unit solid angle; then

$$n_b = \frac{(dL/d\Omega)}{R^2 c^3 \Gamma_{\max}^2 m_p}. \quad (88)$$

The  $\alpha$ -particles are spalled by neutrons with rate  $\dot{Y}_\alpha \approx Y_\alpha Y_n n_b \sigma_{\text{sp}} c$  and their lifetime in the ejecta frame is  $\tau_{\text{life}} = (Y_n n_b \sigma_{\text{sp}} c)^{-1}$ ,

$$\tau_{\text{life}} = \frac{R^2 \Gamma_{\max}^2 m_p c^2}{(dL/d\Omega) Y_n \sigma_{\text{sp}}}. \quad (89)$$

It should be compared with the time of side expansion in the ejecta frame,  $(R/c\Gamma_{\max})$ . If  $\tau_{\text{life}} < (R/c\Gamma_{\max})$  at  $R = R_0$  then most of the  $\alpha$ -particles are disrupted by the internal shocks. This condition reads

$$\Gamma_{\max} < \left[ \frac{A Y_n \sigma_{\text{sp}} (dL/d\Omega)}{2 \lambda_0 m_p c^3} \right]^{1/5} \approx 300 Y_n^{1/5} \left( \frac{dL/d\Omega}{10^{52}} \right)^{1/5} \left( \frac{\lambda_0}{3 \times 10^6} \right)^{-1/5}. \quad (90)$$

#### 4.2.2. $\alpha$ - $\alpha$ collisions

The  $\alpha$ -particles acquire random energy  $(A^2/2)4m_p c^2$  in internal shocks, which is above the spallation threshold. The condition  $\tau_{\text{life}} < (R/c\Gamma_{\max})$  for efficient  $\alpha$ - $\alpha$  spallation is similar to equation (90) (with  $Y_n$  replaced by  $Y_\alpha$ ). There is, however, one more condition. The  $\alpha$ -particles are cooled by Coulomb interactions with  $e^-$  (or  $e^+$ ) on a timescale  $\tau_{\text{Coul}}$ , and efficient spallation requires  $\tau_{\text{life}} < \tau_{\text{Coul}}$  in addition to  $\tau_{\text{life}} < (R/c\Gamma_{\max})$ .

The  $e^\pm$  can be considered as targets at rest for the hot ions because their radiative losses (synchrotron and/or inverse Compton) are rapid compared to the expansion rate. In the fluid frame, the ions with mass  $m_i$ , charge  $Ze$ , and a thermal velocity  $\tilde{\beta}$  loose their energy on timescale (Ginzburg & Syrovatskii 1964)

$$\tau_{\text{Coul}} = \frac{\tilde{\beta}^3 m_i}{3 Z^2 \ln \Lambda \sigma_T m_e c n_e}, \quad (91)$$

where  $n_e = n_- + n_+$  is the total density of  $e^-$  and  $e^+$ , and  $\ln \Lambda \approx 20$  is Coulomb logarithm. The internal shocks give  $\tilde{\beta} \approx A$ . For  $\alpha$ -particles ( $m_i = 4m_p$ ,  $Z = 2$ ), we find that  $\tau_{\text{life}} < \tau_{\text{Coul}}$  requires

$$\frac{n_e}{n_\alpha} < \frac{2A^3}{3 \ln \Lambda} \frac{m_p \sigma_{\text{sp}}}{m_e \sigma_{\text{T}}} \approx 10A^3. \quad (92)$$

This condition is satisfied when helium abundance is high and  $e^\pm$  abundance is low. The postshock matter emits radiation, and  $e^\pm$  pairs can be produced by  $\gamma$ -rays ( $\gamma + \gamma \rightarrow e^- + e^+$ ) that have energy  $h\nu > m_e c^2$  in the ejecta frame. A maximum pair density is evaluated assuming that all the emitted photons above the threshold are converted into pairs. The energy density of these photons,  $w_1$ , is a fraction  $f < 1$  of the total radiation energy,  $w_\gamma = \eta(A^2/2)n_b m_p c^2$ , where  $\eta < 1$  is the radiative efficiency of the shocks. Then

$$\frac{n_\pm}{n_b} \approx \frac{w_1}{n_b m_e c^2} = f\eta \frac{A^2}{2} \frac{m_p}{m_e}. \quad (93)$$

Hence, the Coulomb losses of  $\alpha$ -particles on  $e^\pm$  will prevent the efficient  $\alpha$ - $\alpha$  spallation if  $f\eta > 0.01$ . Note, however, that even in this case a fraction  $\tau_{\text{Coul}}/\tau_{\text{life}} \approx (0.01/f\eta)$  of the  $\alpha$ -particles is disrupted. This is at least 10% as  $f\eta$  is unlikely to exceed 0.1. The released neutrons will contribute to further spallation of helium.

Equation (93) assumes that all photons above the threshold are converted into pairs, which is a reasonable assumption if the optical depth for  $\gamma - \gamma$  interactions  $\tau_{\gamma\gamma} > 1$ . Approximately,  $\tau_{\gamma\gamma} \approx 0.1(w_1/m_e c^2)\sigma_{\text{T}}R/\Gamma_{\text{max}}$ , which yields

$$\tau_{\gamma\gamma} \approx 0.1f\eta \frac{A^2}{2} \frac{m_p}{m_e} n_b \sigma_{\text{T}} \frac{R}{\Gamma_{\text{max}}}. \quad (94)$$

It is easy to show that  $f\eta > 10^{-3}$  ensures  $\tau_{\gamma\gamma} > 1$  at all radii where efficient  $\alpha - \alpha$  spallation can take place [i.e. where  $\tau_{\text{life}} < (R/c\Gamma_{\text{max}})$ ].

## 5. Conclusions

1. The Urca process operates in GRB central engines and establishes an equilibrium  $Y_e = n_p/(n_n + n_p)$ . For bursts fed by accretion, the equilibrium  $Y_e$  is established at accretion rates  $\dot{M} > \dot{M}_{\text{eq}} \approx 10^{31}(M/M_\odot)^{6/5}$  g/s (eq. 46).

2. Neutrino-transparent engines have a neutron excess ( $Y_e < 0.5$ ) if their electron chemical potential  $\mu > Q/2$ , where  $Q = (m_n - m_p)/m_e = 2.53$ . A similar condition for  $\nu$ -opaque engines reads  $\mu > Q$ . This defines a “neutronization” temperature  $T_n$  (eqs. [14] and [23]) below which matter has a neutron excess, and we find  $T < T_n$  for plausible GRB parameters. In particular, accretion-disk engines are neutron rich at  $\dot{M} > \dot{M}_n \approx 10^{31}(M/M_\odot)^2$  g/s (eq. 48).

3. Fireballs produced by neutron-rich engines are also neutron rich. In the case of a  $\nu$ -transparent engine, de-neutronization takes too long time compared to the dynamical time of the

fireball. In the  $\nu$ -opaque case, the neutrino flux from the engine can change  $Y_e$  in the escaping fireball, however, the resulting value is still below 0.5.

4. As the fireball expands and cools, the initially free nucleons tend to combine into helium. This process competes, however, with rapid expansion and can freeze out. The outcome of the competition depends on the fireball collimation. Radial fireballs convert less than half of baryons into helium ( $X_\alpha < 0.5$ ) if their photon-to-baryon ratio  $\phi > 3 \times 10^4 (r_0/3 \times 10^6 \text{ cm})^{0.8}$ , where  $r_0$  is the size of the central engine. In fireballs with parabolic collimation,  $X_\alpha < 0.5$  if  $\phi > 8 \times 10^5 (r_0/3 \times 10^6 \text{ cm})$ . The typical GRB parameters  $\phi \sim 10^5$  and  $r_0 \sim 3 \times 10^6 \text{ cm}$  are just marginal for nucleosynthesis.

5. Deuterium is next abundant element after the free nucleons and helium. Its mass fraction is a few per cent. The abundances of tritium,  $^3\text{He}$ , and heavy elements (mass number greater than 4) are negligible.

6. Even in the extreme case of maximum helium production, there are still leftover neutrons because of the neutron excess,  $Y_e < 0.5$ . The corresponding minimum neutron fraction is  $X_n = 1 - 2Y_e$ .

7. Synthesized helium can be spalled later on. There are at least two possible mechanisms of spallation: (1) n- $\alpha$  collisions with a relative velocity  $\tilde{\beta} > \tilde{\beta}_{\text{sp}} \approx 0.1$  take place before the end of the fireball acceleration if  $\phi > 4 \times 10^5 (L_{\text{th}}/L)^{3/4}$ . This mechanism works for fireballs with Lorentz factors  $\Gamma_{\text{max}} > 200$  (eq. 85). (2) Energetic n- $\alpha$  and  $\alpha$ - $\alpha$  collisions occur when the ejecta are heated by internal shocks. This mechanism can be efficient at modest  $\Gamma_{\text{max}} \lesssim 300$  (eq. 90).

At the final stages of the preparation of this manuscript, a paper by Puet, Woosley, & Hoffman (2002) appeared. They evaluate  $Y_e$  for numerical accretion models of Popham et al. (1999). The results are consistent with our analysis in § 2 (taking into account that Popham et al. models have  $M = 3M_\odot$  and a slightly different definition of the viscosity parameter — our  $\alpha$  is smaller by a factor of 2/3).

I thank Raymond Sawyer for discussions of the neutronization process and Matthias Liebendorfer for an introduction to the Lattimer-Swesty Equation of State. I acknowledge the hospitality of the ITP at Santa Barbara, where part of this work was done. This research was supported by NSERC, and in part by the NSF grant PHY99-07949 and RFBR grant 00-02-16135.

## REFERENCES

- Bahcall, J. N., & Mészáros, P. 2000, Phys. Rev. Lett., 85, 1362  
 Balbus, S. A., & Hawley, J. F. 1998, Rev. Mod. Phys., 70, 1  
 Beloborodov, A. M. 2000, ApJL, 539, 25L

- Beloborodov, A. M. 2002, *ApJL*, submitted, astro-ph/0209228
- Bulik, T., Sikora, M., & Moderski, R. 2002, astro-ph/0209339
- Derishev, E. V., Kocharyan, V. V., Kocharyan, Vl. V. 1999, *ApJ*, 521, 640
- Di Matteo, T., Perna, R., & Narayan, R. 2002, astro-ph/0207319
- Esmailzadeh, R., Starkman, G. D., & Dimopoulos, S. 1991, *ApJ*, 378, 504
- Fuller, G. M., Puet, J., & Abazajian, K. 2000, *Phys. Rev. Lett.*, 85, 2673
- Ginzburg, V. L., & Syrovatskii, S. I. 1964, *The Origin of Cosmic Rays*, Oxford: Pergamon
- Kohri, K., & Mineshige, S. 2002, *ApJ*, 577, 311
- Landau, L. D., & Lifshitz, E. M. 1980, *Statistical Physics*, Pergamon Press, Oxford
- Lattimer, J. M., & Swesty, F. D. 1991, *Nucl. Phys. A*, 535, 331
- Lemoine, M. 2002, *A&A*, 390, L31
- MacFadyen, A. I., & Woosley, S. E. 1999, *ApJ*, 524, 262
- Mészáros, P. 2002, *ARA&A*, 40, 171
- Mészáros, P., & Rees, M. J. 2000, *ApJ*, 541, L5
- Mészáros, P., & Rees, M. J. 2001, *ApJ*, 556, L37
- Meyer, B. S. 1994, *ARA&A*, 32, 153
- Narayan, R., Piran, T., Kumar, P. 2001, *ApJ*, 557, 949
- Popham, R., Woosley, S. E., & Fryer, C., 1999, 518, 356
- Puet, J., Abazajian, K., & Fuller, G. M. 2001, 64
- Puet, J., Guiles, S., & Fuller, G. M. 2002, astro-ph/0205056
- Puet, J., & Dalal, N. 2002, *ApJ*, 573, 770
- Puet, J., Woosley, S. E., & Hoffman, R. D. 2002, astro-ph/0209412
- Qian, Y.-Z., Fuller, G. M., Mathews, G. J., Mayle, R. W., Wilson, J. R., & Woosley, S. E. 1993, *Phys. Rev. Lett.*, 71, 1965
- Rees, M. J., & Mészáros, P. 1994, *ApJ*, 430, L93
- Ruffert, M., Janka, H.-T., Takahashi, K., & Schaefer, G. 1997, *A&A*, 319, 122
- Smith, M. S., Kawano, L. H., & Malaney, R. A. 1993, *ApJ*, 85, 219
- Wagoner, R. V., Fowler, W. A., & Hoyle, F. 1967, *ApJ*, 148, 3